IN-29

186490

74P

NASA Contractor Report 191527

The Feasibility of Producing Aluminum-Lithium Structures for Cryogenic Tankage Applications by Laser Beam Welding

R. P. Martukanitz
K. G. Lysher

Pennsylvania State University
Applied Research Laboratory
State College, Pennsylvania

NASA

National Aeronautics and
Space Administration

Langley Research Center
Hampton, Virginia 23681-0001

N94-14026

Unclas

G3/29   0186490

(NASA-CR-191527) THE FEASIBILITY
OF PRODUCING ALUMINUM-LITHIUM
STRUCTURES FOR CRYOGENIC TANKAGE
APPLICATIONS BY LASER BEAM WELDING
(Pennsylvania State Univ.) 74 p

ABSTRACT

Laser beam welding offers several potential advantages for producing "built-up" structures from aluminum-lithium alloys for cryogenic tankage applications. These include: improved load transfer between stiffeners and the skin, enhanced structural integrity of welds, higher productivity, lower cost, and processing in a fully automated environment. Based on these potential benefits a program was initiated between NASA Langley Research Center and the Applied Research Laboratory, The Pennsylvania State University (ARL Penn State) to determine the feasibility of laser beam welding aluminum-lithium alloys for cryogenic tankage. Four primary tasks were proposed to determine the viability of laser beam welding for this application. These included establishment of process parameters for two thickness and alloy combinations, production of test specimens, determination of critical weld properties, and fabrication of prototype panels for evaluation. Laser beam welding evaluations were conducted on aluminum-lithium alloy combinations 8090-T6 welded to 2090-T83 and 2095-T6 welded to 2095-T8 to simulate stiffener to skin conditions. Process development, production of test specimens, and fabrication of prototype panels were performed using the Laser Articulating Robotic System serviced by a 14 kW carbon-dioxide laser.
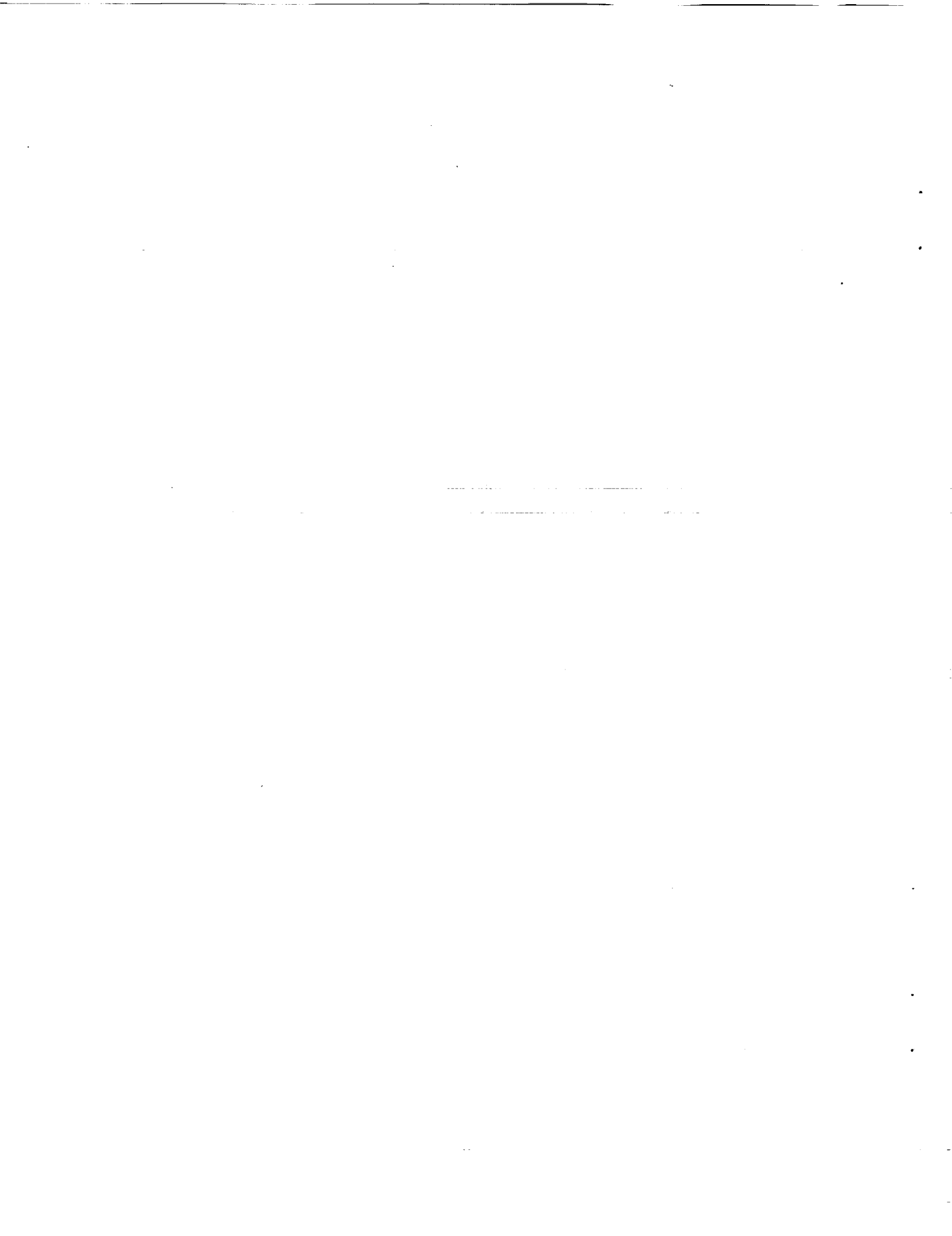
Results of the evaluation indicate that laser beam welding may provide improved productivity and lower costs over resistance welding for fabrication of stiffened panels. Lap-welds having good penetration and positive weld bead reinforcement were produced by autogenously laser beam welding at power levels of 5 to 7 kW and travel speeds of 150 to 160 IPM (6.4 to 6.8 cm/s). Aggressive pretreatment in the form of chemical milling in a 32 percent NaOH aqueous solution at 210°F (99°C) was found to be necessary to reduce porosity at the interface. This required removal of 0.010 in. (0.25 mm) per side by chemical milling prior to welding and is believed due to the presence of a hydrogen-enriched layer near the surface. Although chemical milling was able to reduce porosity at the interface between the stiffeners and skin, radiography indicated that weld porosity was consistently observed at the root of the welds. Adequate clamping force between the stiffeners and face-sheet was also found to be critical in achieving consistent weld quality along the length of the stiffeners.

Conditions amicable to improved load transfer and enhanced structural integrity were also demonstrated by the laser beam welding process. Laser beam welding provided accessibility such that lap-welds could be produced very near the edge of the vertical member on stepped-hat stiffeners of prototype panels. Tensile tests of laser beam welds representing partial penetration of the face-sheet provided a joint efficiency of 77 percent (at 40 percent through-thickness penetration) for 2090-T83 and 65 percent joint efficiency (at 60 percent through-thickness penetration) for 2095-T8. However, it is anticipated that the joint efficiency of the partial penetration welds of the skin would be greater for 2095-T83, based on equal penetration. Results of tension shear tests of lap-welds that were produced by laser beam welding indicated that the alloy combination of 2095-T6 to 2095-T8 exhibited significantly higher weld shear strength at the interface in comparison to welds of 8090-T6 to 2090-T83. This is believed due to the ability of alloy 2095 to precipitation strengthen (naturally age) after welding. The average shear strength of welds between 2095-T6 to 2095-T8 was 18.8 KSI (130 MPa) as compared to an average shear strength of 11.7 KSI (81 MPa) for 8090-T6 welded to 2090-T83. The results of mechanical property characterization indicated that minimal degradation to the base metal may be achieved by laser beam welding.

Based on the results of this initial investigation, it is recommended that further laser beam welding evaluations be conducted. Laser beam welding has demonstrated the ability to offer high production rates, and possibly lower cost, for joining of stiffeners to skin. Extrinsic process development, such as fixture and joint design, should be optimized for laser beam welding of larger prototype panels. Direct comparison of laser beam welded and resistance welded structures should then be performed to ascertain structural integrity, quality, and costs associated with these processes.

TABLE OF CONTENTS

LIST OF FIGURES

LIST OF FIGURES - Continued

LIST OF FIGURES - Continued

LIST OF TABLES

1.0 INTRODUCTION

NASA and industry studies have shown that low density aluminum-lithium alloy technology can aid in improving performance and increase payloads of launch vehicles (Refs. 1-3). Components that have been identified for implementation of these new alloys are the cryogenic tanks used to carry liquid oxygen and liquid hydrogen. An artist's rendition of an advanced launch vehicle showing the liquid oxygen and hydrogen tanks is shown in Figure 1. These tanks, as well as the intertank used to connect the hydrogen and oxygen tanks. are assembled from integrally machined panels containing stiffeners. The tanks may be used in pressure environments ranging from zero to 80.0 psi due to internal pressure loading of the oxidant and fuel under flight dynamics. They will also be used to support the upper vehicle structure and payload which may result in compressive loading ranging from 900 to 3,000 psi. Since the tanks will be used to store cryogenic propellants, the panels may experience temperatures from -460°F to +150°F (-273°C to 66°C).

NASA and industry has proposed the use of "built-up" structures for aluminum-lithium panels which would be fabricated into tanks (Ref. 4). This concept is radically different from the current panel design requiring extensive machining to produce the stiffened structure and results in accumulation of costly aluminum-lithium scrap. Although the recently developed aluminum-lithium alloys offer between 7 to 12 percent reduced density and approximately 10 percent increase in stiffness over the current alloy, 2219-T87, used for these applications, the need for specialized processing has resulted in costs of three-times that of conventional aluminum alloys. Hence, removal of large amounts of material by machining is not a cost-effective approach for utilizing aluminum-lithium alloys for this application.

The built-up concept would utilize net or near-net shapes to form stiffeners that would be joined to skin sheet to produce the panels. Figure 2 depicts a cross-section of one concept for the proposed built-up structure. Longitudinal stiffeners would be produced by methods such as extruding, roll-forming, or superplastically forming (SPF) of parts. Because the SPF process possesses the ability to produce relatively complex shapes, which may result in optimized designs, SPF processing of the stiffeners is especially of interest. The stiffeners would then be joined to the outer skin-sheet, in order to produce the panels. Current methods being evaluated for joining the stiffeners to skin are resistance spot or seam welding. Aluminum-lithium alloys of interest for producing the built-up structure include 2095 (formerly Weldalite™ 049) stiffeners to 2095 skin and alloy 8090 stiffeners to alloy 2090 skin. Nominal compositions, densities, and elastic modulii for these alloys are shown in Table I (Refs. 5-7). As mentioned previously, the stiffeners are necessary along the length of the panels in order to prevent longitudinal buckling during loading of the tank. Compressive stress along the length of the panels would translate into sheer stress at the interface of the stiffener to skin welds, and hoop stress due to internal pressure would result in transverse tensile stress across the partial penetration weld and heat affected zone of the skin.

1

Laser welding for this application possesses several advantages over resistance spot and seam welding. In order to optimize structural integrity during load transfer, it is most desirable to produce the welds as close to the corner of the vertical member of the stiffener as possible. Prototype stiffeners, currently being evaluated, possess approximately a 0.750 (1.9 cm) inch wide flange primarily for resistance spot welding access and results in a weight penalty and waste of expensive material. Laser welding could provide a continuous weld along the length of the extrusion or SPF part extremely close to the corner of the vertical member. Because of this, the flange requirements for laser beam welding of the stiffeners to face-sheet would be greatly reduced.

Laser welding offers other potential benefits such as higher production rates, narrow heat affected zones, and the potential for process automation. Laser welding of lap-joints in the thicknesses currently being considered may employ extremely high welding speeds when compared to current fusion welding techniques. It is estimated that welding speeds of 100 to 200 inches per minute (4.2 to 8.4 cm/s) are achievable by multikilowatt, carbon-dioxide lasers for this application. Because of the extensive amount of welding required to fabricate the panels, higher welding speeds would significantly impact productivity and cost. The high welding velocity in combination with the laser's ability to generate high power densities results in low overall heat input to the base metal. The ramifications of this characteristic is minimal thermal distortion and high joint strength associated with laser beam welds. Figure 3 shows a comparison of ultimate tensile strength of butt-welds in alloy 2090-T83 produced using various welding processes (Refs. 8 and 9). As illustrated in the figure, welds produced with the high-energy density processes such as electron beam and laser beam welding exhibited the highest ultimate tensile strength. However, as opposed to electron beam welding, laser beam welding does not require a vacuum during processing. The favorable weld strength exhibited by laser beam welds is primarily due to the high cooling rates in the fusion zone and adjacent base material. Finally, for safety considerations laser beam welding requires automated manipulation of either the beam or the part, as well as automatic control of the various processing parameters. Since laser beam welding is performed in a fully automated processing environment it provides inherent capabilities for process control.

Based on the potential benefits of laser beam welding for fabrication of the stiffened panels, a program was initiated between NASA Langley Research Center and the Applied Research Laboratory, The Pennsylvania State University (ARL Penn State) to determine the feasibility of laser beam welding aluminum-lithium alloys for cryogenic tankage. Four primary tasks were proposed to determine the viability of laser beam welding for this application. This included establishment of process parameters for two thickness and alloy combinations, production of test specimens, determination of critical weld properties, and fabrication of prototype panels for evaluation. The sequence of tasks for the program is shown in Figure 4.

Process parameters would be established to provide lap welds possessing positive weld reinforcement with partial penetration in the face-sheet and at processing speeds applicable to high production rates for two face-sheet thicknesses and two alloy combinations. Welding parameters would be developed utilizing the Laser Articulating Robotic System (LARS) at ARL Penn State, which is serviced by a 14 kW United Technologies carbon dioxide laser. LARS provides full process automation while being capable of producing prototype panels up to 10 ft. by 10 ft. (3.0 m by 3.0 m) in size. A schematic of LARS is shown in Figure 5.

2.0 EVALUATIONS

The evaluation involved four primary tasks: process parameters development, production of test specimens, characterization of test specimens, and fabrication of prototype panels. Processing parameters, such as beam power, travel speed, and shielding gas arrangement would be identified for producing lap-welds using LARS. Constraints imposed in producing the lap-welds were positive weld-bead reinforcement and approximately 50 percent penetration into the face-sheet at processing speeds applicable to high production rates. Also of consideration during this task would be pretreating procedures for the aluminum-lithium alloys. Because aluminum-lithium alloys possess a hydrogen-enriched layer near the surface due to thermally induced oxidation during primary processing, surface pretreatments would be concurrently evaluated during process development with the goal of producing porosity-free welds (Refs. 10 and 11). Once established, these processing parameters would be used to produce test specimens for determining weld characteristics critical for ascertaining the viability of laser beam welding for this application.

Mechanical analysis indicated that during service, the weld joints of the built-up panels would incur two primary loading conditions. Compressive stress along the length of the panels would translate to shear stress at the weld between the stiffener to skin, and hoop stress due to internal pressure would result in transverse tensile stress across the partial penetration and heat affected zone of the skin. Based on this analysis, it was recognized that shear strength of the lap weld and strength across the partial penetration of the skin would be essential for determining the viability of laser beam welding. This resulted in a testing plan that would utilize specimens produced using optimal processing parameters to determine critical joint properties. Results of static tests would then be compared to prototype panels tested under simulative loading conditions.

Material required for program execution was supplied by NASA Langley Research Center. This included sheet material of alloys 2095-T6 and 8090-T6 representing stiffeners, 2095-T8 and 2090-T83 representing skin-sheet, as well as SPF stepped-hat stiffeners of 2095-T5 and 8090-T5. The alloy and thickness combinations for stiffeners and skin that were initially of interest are shown in Table II.

2.1 Process Parameters Development

Welding parameters were developed on LARS, which is serviced by a 14 kW, United Technologies Industrial Lasers Model SM21-14, carbon dioxide laser. LARS is a large rectilinear robot having three linear degrees-of-freedom and three rotational degrees-of-freedom. The system utilizes water-cooled, copper mirrors to manipulate the unfocused beam, being approximately 3.0 in. (7.6 mm) in diameter, to the welding head. A spherical, water-cooled mirror is then used to focus the beam to a spot size of approximately 0.030 inch (0.8mm) in diameter. This results in attainable power densities at focus of 7.07×10^6 w/in.^{2} (1.1×10^6 w/cm^2) at 5 kW to 1.99×10^7 w/in.^{2} (3.08×10^6 w/cm^2) at 14 kW. The reflective optics utilized on LARS provide an ample stand-off distance between the work-piece and welding head; therefore, shielding gas is typically supplied externally through the use of a copper nozzle. A schematic of the optical arrangement utilized for LARS is shown in Figure 6.

3

2.1.1 Initial Process Development

Initial process parameters were obtained by producing autogenous lap-welds on thicknesses applicable to the stiffener to skin configuration with material in the as-received condition. All material was received in the as-fabricated condition except for the 0.050 in. (1.3 mm) thick 8090-T6 sheet that was given an acid pretreatment (8 oz. of commercial Aluma™ etchant per gallon of water at room temperature for 10 minutes) at NASA Langley Research Center. The two thickness combinations were: 0.050 in. (1.3 mm) thick top-sheet to a 0.095 in. (2.4 mm) thick bottom-sheet, and 0.050 in. (1.3 mm) thick top-sheet to a 0.120 in. (3.0 mm) thick bottom-sheet. Sheet specimens 4.0 in. (10.2 cm) in width and 6.0 in. (15.2 mm) in length were completely overlapped and welded at the center along the length direction. Clamping of the sheets was accomplished through the use of two 0.250 in. (6.4 mm) thick by 1.5 in. (3.8 cm) wide by 8.0 in. (20.3 cm) long bars of Inconel 625 allowing a 1.0 in. (2.5 cm) gap along the center of the sheet for welding. The Inconel 625 bars were deformed to obtain a slight curvature, and with the curvature facing upward the bars were clamped at three points along the length of the sheet specimens. A bronze plate machined to 0.375 in. (9.5 mm) in thickness was used as backing beneath the thicker bottom-sheet. Figure 7 depicts the clamping arrangement used during this evaluation.

Full penetration of the top-sheet and partial penetration of the bottom-sheet was achieved at power levels of 6.5 to 7.0 kW and travel speeds of 150 to 170 IPM (6.4 to 7.2 cm/s). A stand-off distance of approximately 6.0 in. (15.2 cm) between the welding head and the part was utilized. Helium shielding gas at a flow rate of 200 CFH (94.4 l/min.) was supplied by a 0.375 in. (9.5 mm) inside-diameter nozzle mounted at a 35° angle from the vertical and directed at the front edge of the weld pool opposite the welding direction. These parameters were used to produce autogenous welds having bead widths of approximately 0.187 in. (4.7 mm) and exhibiting positive weld bead reinforcement. Operating within the range of parameters shown above provided approximately 75 percent penetration for both alloy combinations. The welding parameters identified during initial process development are summarized in Table III.

2.1.2 Factorial Experiment

After establishing initial process parameters, a 2^3 factorial experiment was designed to measure the effects of alloy combination, material thicknesses, and precleaning processes on weld porosity. This involved eight combinations for a total of 16 runs with replication. Values of plus-one or minus-one were arbitrarily assigned to the conditions for each independent variable. The experimental conditions were:

1)	Alloy Combinations:	(-1)	8090-T6 to 2090-T83
		(+1)	2095-T6 to 2095-T8
2)	Material Thicknesses:	(-1)	0.050 inches to 0.095 inches (1.3 to 2.4 mm)
		(+1)	0.050 inches to 0.120 inches (1.3 to 2.4 mm)
3)	Cleaning Treatment:	(-1)	Chemically cleaned in sodium hydroxide
		(+1)	Wire brushed and solvent degreased

4

Pretreating techniques utilized in the factorial experiment were chemical cleaning by immersion in a 8% NaOH solution at 170 °F (77 °C) for 60 minutes to remove 0.001 in. (0.02 mm) per side and mechanically wire brushing followed by cleaning with acetone just prior to welding. The chemically etched specimens were wrapped in paper, stored at ambient temperature, and welded within 48 hours of treatment. The mechanically wire brushed samples were also welded within 48 hours of treatment. Welding parameters were adjusted during the experiment to obtain a constant depth of penetration of 75 percent and varied from 6.5 to 7.0 kW beam power and 150 to 170 IPM (6.4 to 7.2 cm/s) travel speed.

Four-inch (10.2 cm) long autogenous lap-welds were produced on specimens representing the various combinations. The clamping arrangement used during the factorial experiment was identical to the arrangement described earlier. After welding, a cross-section and a 1.0 in. (2.5 cm) long longitudinal section from each weld were removed and prepared for metallographic analysis. A section 1.2 in. (3.2 cm) in length from each weld was also peel-fractured at the weld interface and examined at 10X magnification for weld porosity. The fractured lap-welds were characterized by determining the number of pores less than 0.005 in. (0.13 mm) in diameter, between 0.005 and 0.020 in. (0.13 and 0.51 mm) in diameter, and greater than 0.020 in. (0.51 mm) in diameter. The values obtained for the initial run and replication were averaged for the three pore-size categories. Results of the factorial experiment showing distribution of porosity, based on the average of two 1.2 in. (3.2 cm) long weld specimens, along with experimental conditions are shown in Table IV.

2.1.3 Second Process Parameters Evaluation

It was observed during initial process development that penetration depth into the bottom-sheet was effected by the alloy combination being welded. The alloy combination of 8090-T6/2090-T83 required less heat input than 2095-T6/2095-T8 to obtain a given penetration depth. Therefore, it was necessary to adjust welding parameters to obtain equal penetration depths for each alloy combination. Modifications to the welding parameters were made by slightly adjusting travel speed and power to obtain 50 percent penetration into the bottom-sheet for both alloy combinations. Specimen configuration and clamping arrangement used during the second process parameters development were identical to those described earlier. The combination of 8090-T6/2090-T83 necessitated lower beam power and higher welding speeds. The modified parameters established for each alloy and thickness combination are shown in Table V.

2.1.4 Chemical Cleaning Evaluations

Earlier evaluations conducted during process development had indicated that unacceptable porosity was formed within the fusion zone during laser beam welding while employing pretreatments such as wire brushing, solvent degreasing, and mild NaOH etching. Metallographic sections taken longitudinally along the weld continued to show porosity within the fusion zone. It was believed that a hydrogen enriched layer near the surface of the base metal was responsible for generating gas porosity during welding, and this theory had been supported by results of prior investigations using conventional welding processes (Refs. 12-14). To determine if a hydrogen enriched layer was responsible for generating the weld

5

porosity, more aggressive pretreating was evaluated. Vendors were contacted to obtain quotes for chemical treating of specimens to remove up to 0.010 in. (0.25 mm) per side by chemical milling in NaOH aqueous solutions. Two vendors were chosen for evaluating the effect of chemical milling on weld porosity. These were: Chem-Tron Company of Danbury, CT and Chemtronics Corporation of El Cajon, CA.

Initial samples were forwarded to Chem-Tron Company requesting 0.010 in. (0.25 mm) to be removed per side; however, inspection of the returned samples indicated that 0.001 in. (0.02 mm) per side was. removed. These specimens were treated by chemical milling in a 20 percent NaOH solution at 81 °F (27°C) for 45 minutes. An evaluation was conducted on the material chemically milled at Chem-Tron. Autogenous laser beam welded specimens of both alloy and thickness combinations were produced using the established parameters shown in Table V. Treated material was wrapped in paper and stored at ambient temperature; welding was performed within 48 hours of chemical milling. If successful in producing porosity-free welds, the panels produced during the experiment would also be utilized to determine weld strength across the partial penetration welds of the face-sheet. Specimen configuration utilized during the evaluation was two 4.0 in. by 6.0 in. (10.2 by 15.2 cm) sheets having complete overlap with the laser weld at the center along the 6.0 inch (15.2 cm) dimension. Clamping arrangement remained the same as described previously. After welding, the first and last inch (2.5 cm) of weld was removed and discarded. Additional samples were removed for metallographic analysis. The remaining panel being approximately 4.0 in. by 3.0 in. (10.2 by 7.6 cm) was retained for tensile test specimens of the partial penetration welds of the bottom sheet, representing alloys 2090-T83 and 2095-T8.

The panels retained for tensile tests were prepared by carefully machining-away the top sheet, being alloy 8090-T6 or 2095-T6, to within 0.003 in. (0.08 mm) of the bottom sheet. The remaining weld crown was then removed by hand-sanding to achieve flat panels suitable for obtaining subsize tensile specimens having a 1.0 in. (2.5 cm) gage length with the weld transverse to the specimen. However, during the finishing operation it became apparent that unacceptable porosity was present at the interface. The interface of both the 0.095 and 0.120 in. (2.4 and 3.0 mm) thick panels of 2905 exhibited large pores approximately 0.010 to 0.030 in. (0.25 to 0.76 mm) in diameter along the length of the weld; whereas, the weld on alloy 2090-T8 exhibited smaller pores approximately 0.003 to 0.010 in. (0.08 to 0.25 mm) in diameter. The panels were dye penetrate inspected to readily illustrate the porosity present along the weld. Based on these results, production of tensile specimens for measuring strength across the partial penetration weld of the face-sheet was postponed until an acceptable pretreating method was identified.

Based on the laser welding results of material that had been chemically milled 0.001 in. (0.03 mm) per side by Chem-Tron Company of Danbury, CT, specimens representing both alloy and thickness combinations were forwarded to Chemtronics Corporation, El Cajon, CA for chemical milling to remove 0.005 and 0.010 in. (0.13 mm and 0.25 mm) per side. Specimens were chemically milled by Chemtronics Corporation by immersion in a 32 percent NaOH aqueous solution at 210°F (99°C) for 5 to 10 minutes. Thickness measurement were performed on material prior to shipment and after return from Chemtronics Corporation to confirm the amount of material removed by chemical milling. The samples were then welded using the specimen configuration and clamping arrangement described earlier; however, because of the decrease in thickness and change in surface conditions, slight adjustment were made to the pre-established welding parameters. Treated material was wrapped in paper and stored at ambient temperature. Welds were performed within 48 hours of chemical milling. The parameters used

to produce the panels are shown in Table VI. These parameters provided between 35 and 70 percent partial penetration to the thicker, bottom-sheet.

After welding the material that had been chemically milled by Chemtronic Corporation to remove 0.005 and 0.010 in. (0.13 and 0.25 mm) per side, the first and last half-inch (12.7 mm) of weld was removed and discarded. Additional samples were removed for metallographic analysis to determine weld penetration. The remaining panels being approximately 4.0 in. by 3.5 in. (10.2 by 8.9 cm) in size were retained for obtaining tensile test specimens of the partial penetration welds of the bottom sheet, representing alloys 2090-T83 and 2095-T8. As performed earlier, the panel retained for tensile test specimens was prepared by carefully machining-away the top sheet, being alloy 8090-T6 or 2095-T6, to within 0.003 in. (0.08 mm) of the bottom sheet. The remaining weld crown was then removed by hand-sanding to achieve flat panels suitable for obtaining subsize tensile specimens.

Identical to the procedure utilized for the welds produced from material chemically milled 0.001 in. (0.02 mm) per side by Chem-Tron Company, the 4.0 in. by 3.5 in. (10.2 by 8.9 cm) panels that had been prepared for tensile testing of the partial penetration welds of the bottom sheet were also used to determine the extent of porosity associated with the welds. The top surface of the panels provided a view of the weld that was present at the interface between the top and bottom sheets. The amount of porosity exhibited at the interface could be directly related to the degree of chemical milling performed on the sheets prior to laser beam welding.

The level of porosity at the interface associated with the welds produced from material that was chemically milled by Chemtronic Corporation to remove 0.005 and 0.010 in. (0.13 and 0.25 mm) per side was quantified by visually determining the number of pores present per linear inch of weld at a 10X magnification. This was also performed on panels chemically treated by Chem-Tron Company representing material that was chemically milled 0.001 in. (0.02 mm) per side. These measurements represented the amount of porosity per inch over a total of 7.0 in. (17.8 cm) of weld. The results of these determinations are shown in Figure 8 and support the supposition that elimination of the hydrogen enriched layer by removing 0.010 in. (0.25 mm) per side dramatically reduced porosity at the weld interface. The panels were also dye penetrant inspected to readily illustrate the amount of porosity present along the weld. Photographs of the weld interface of the welded panels representing the 0.120 in. (3.0 mm) thick bottom-sheet that were produced from the material chemically milled 0.001 in. (0.02 mm) per side by Chem-Tron Company and chemically milled 0.005 and 0.010 in. (0.13 and 0.25 mm) per side by Chemtronics Corporation after dye penetrant inspection are shown in Figures 9 and 10.

2.2 Production of Test Specimens

Autogenous welds were produced on lap-configurations selected to simulate stiffener to skin conditions for determination of critical properties. Critical properties that were of interest included strength across the partial penetration welds of the skin and shear strength at the weld interface between the stiffener and skin. Results of the chemical pretreating evaluations had indicated that chemical milling of material was required to produce welds having minimal porosity at the interface. Therefore, material that was utilized for producing test specimens was chemically milled to remove either 0.005 in. or 0.010 in. (0.13 or 0.25

mm) per side prior to welding. The thicknesses discussed below represent material thicknesses prior to chemical milling. Panels of 0.050 in. (1.3 mm) thick sheet welded to 0.120 in. (3.0 mm) thick sheet that had both been chemically milled 0.010 in. (0.25 mm) per side for each alloy combination were used for measuring strength across the partial penetration welds of the skin, the 0.120 in. (3.0 mm) thick material.

For weld shear strength determinations it was decided that the effect of chemical milling on weld porosity, and hence shear strength at the weld interface, be ascertained. Therefore, material that was chemically milled 0.001 in., 0.005 in., and 0.010 in. (0.02, 0.13, and 0.25 mm) per side was used to produce weld shear strength specimens. Since chemical milling of 0.010 in. (0.25 mm) per side dramatically reduced the thickness of the 0.050 in. (1.3 mm) thick material used to simulate the stiffeners, additional sheet material of 2095-T6 being 0.068 in. (1.7 mm) in thickness was obtained for producing weld shear strength specimens. Thicker sheet of 8090-T6 was not readily available; therefore, the original 0.050 in. (1.3 mm) thick 8090-T6 material was utilized to produce weld shear strength samples for the combination of 8090-T6 to 2090-T83.

2.2.1 Specimens for Determining Strength Across Partial Penetration

The panels representing the 0.050 in. (1.3 mm) thickness to 0.120 in. (3.0 mm) thickness produced from the material chemically milled to remove 0.010 in. (0.25 mm) per side by Chemtronics Corporation were utilized for obtaining mechanical properties across the partial penetration welds of the bottom sheet. This condition was chosen because the welds produced from the material that had been chemically milled to remove 0.010 in. (0.25 mm) per side prior to welding exhibited minimal porosity at the interface. After carefully removing the top-sheet, tensile test specimens were removed from the bottom sheet representing the partial penetration welds on the 0.120 in. (3.0 mm) thick 2090-T83 and 2095-T8 material. Five test samples 0.50 in. (12.7 mm) in width were removed from samples B1 (representing the 0.120 in. thick 2090-T83) and B4 (representing the 0.120 in. thick 2095-T8). The welds were at the center of the samples and transverse to the direction of testing. Three additional samples of the 0.120 in. (3.0 mm) thick 2090-T83 and 2095-T8 that had not been welded were also obtained for base metal strength determinations. The base metal samples represented material that was not chemically milled.

2.2.2 Welds Shear Strength Specimens

Weld shear strength specimens were produced on material that had been chemically milled 0.001, 0.005, and 0.010 in. (0.02, 0.13, and 0.25 mm) per side to ascertain the effect of porosity on weld shear strength. Material representing the thicknesses and alloys of interest for simulating the stiffener to skin welds were forwarded to Chemtronics Corporation, El Cajon, CA for chemical milling. Sheet specimens 4.0 by 6.0 in. (10.2 by 15.2 cm) in size and representing 0.050 in. (1.3 mm) thick 8090-T6, 0.068 in. (1.7 mm) thick 2095-T6, 0.095 and 0.120 in. (2.4 and 3.0 mm) thick 2090-T83, and 0.095 and 0.120 in. (2.4 and 3.0 mm) thick 2095-T80 were forwarded to Chemtronics Corporation. As discussed previously, it was decided to utilize the 0.068 in. (1.7 mm) thick 2095-T6 material in lieu of the 0.050 in. (1.3 mm) thickness due to the relatively large amount of material that would be removed by chemical milling. Thicker sheet of 8090-T6 was not readily available; therefore, the 0.050 in. (1.3 mm) thick

8090-T6 was utilized for producing weld shear strength specimens for the 8090-T6 to 2090-T83 combination. Specimens were chemically milled by immersion in a 32 percent NaOH aqueous solution at 210°F (99°C) for 1 to 10 minutes. Thickness measurements were performed on material prior to shipment and after return from Chemtronics Corporation to confirm the amount of material removed by chemical milling. The milled specimens were wrapped in paper and stored at ambient temperature prior to welding.

After chemical milling of the material weld specimens were produced for obtaining weld shear strength at the interface. The 4.0 by 6.0 in. (10.2 by 15.2 cm) panels were welded to produce an autogenous lap-weld along the center of a 4.0 (10.2 cm) overlap. The weld specimen configuration used for obtaining weld shear strengths are shown in Figure 11. Three welded panels were produced for each thickness and alloy combination having 0.001, 0.005, and .010 in. (0.02, 0.13, and 0.25 mm) removed per side by chemical milling prior to welding. Clamping of the sheet during welding was similar to the arrangement discussed earlier. A stand-off distance of approximately 6.0 in. (15.2 cm) between the welding head and the part was utilized. Helium shielding gas at a flow rate of 200 CFH (94.4 l/min.) was supplied by a 0.375 in. (9.5 mm) inside-diameter nozzle mounted at a 35° angle from the vertical and directed at the front edge of the weld pool opposite the welding direction. Welding parameters used to produce the partial penetration welds were also utilized for producing the shear strength specimens; however, minor changes in beam power were made based on depth of penetration observations from weld cross-sections. Parameters were adjusted to obtain a nominal penetration of 50 percent into the bottom-sheet. Welding parameters utilized for these specimens are shown in Table VII and Table VIII for the 8090-T6 to 2090-T83 and 2095-T6 to 2095-T8 combinations, respectively.

2.3 Characterization

Characterization of laser beam welds entailed determining critical mechanical properties necessary for determining the viability of the process for cryogenic tankage applications and limited metallurgical analysis. Strength across the partial penetration weld of the face-sheet and weld shear strength at the interface were considered critical for ascertaining the applicability of the process. Metallurgical analysis was used to support the results of mechanical property testing. This included measuring the natural aging response of the fusion zone and heat affected zone for both alloy combinations and the examination of fracture surfaces of mechanical property samples.

2.3.1 Mechanical Property Characterization

The panels produced during the chemical pretreating evaluation representing the 0.120 in. (3.0 mm) thick bottom-sheets of 2090-T83 and 2095-T8 were utilized for obtaining strengths across the partial penetration welds. These samples were forwarded to Westmoreland Mechanical Testing Laboratory, Latrobe, PA for transverse determinations of ultimate tensile strength, yield strength, and percent elongation associated with the partial penetration welds in the 2090-T83 and 2095-T8 bottom-sheet. Subsize mechanical property specimens, having a 1.0 in. (2.5 cm) gage length with the weld transverse to the specimen, were machined from the samples. This resulted in tensile test specimens having a reduced section width of

9

0.50 in. (1.3 cm) and a 1.0 in. (2.5 cm) gage length for material representing partial penetration welds in 0.120 in. (3.0 mm) thick 2090-T83 and 2095-T8, as well as unwelded base metal. Tensile testing of the subsize specimens was conducted according to ASTM Specification E8. A minimum period of 220 hours elapsed between welding and testing to ensure that sufficient precipitation strengthening (natural aging) in the fusion zone and heat affected zone had occurred. Results of the tensile tests across the partial penetration welds of 2090-T83 and 2095-T8, as well as base metal strengths, are shown in Table IX and Table X, respectively.

Welded specimens representing both alloy and thickness combinations that had been chemically milled 0.001, 0.005, 0.010 in. (0.02, 0.13, and 0.25 mm) per side prior to welding were sectioned to obtain samples for weld shear strength determinations. One-inch (2.5 cm) wide sections were removed from the welded panels with the lap-weld at the middle of the section and transverse to the length. These sections were then machined to provide samples being 0.750 in. (1.91 cm) wide and 7.75 in. (19.7 cm) long. Samples representing 0.050 in. (1.3 mm) thick 8090-T6 to 0.095 in. (2.4 mm) thick 2090-T83 and 0.068 in. (1.7 mm) thick 2095-T6 to 0.095 in. (2.4 mm) thick 2095-T8 were forwarded to NASA Langley Research Center for determination of weld shear strengths. Samples representing 0.050 in. (1.3 mm) thick 8090-T6 to 0.120 in. (3.0 mm) 2090-T83 and 0.068 in. (1.7 mm) thick 2095-T6 to 0.120 in. (3.0 mm) thick 2095-T8 were retained by ARL Penn State for testing .

Shear strength testing of ARL Penn State samples representing 0.050 in. (1.3 mm) thick 8090-T6 to 0.120 in. (3.0 mm) thick 2090-T83 and 0.068 in. (1.7 mm) thick 2095-T6 to 0.120 in. (3.0 mm) thick 2095-T8 was performed at Westmoreland Mechanical Testing Laboratory, Latrobe, PA. The shear area was obtained by measuring the weld width at the interface on the edges of the samples and the length of the weld prior to shipment to Westmoreland Mechanical Testing Laboratory. A width measurement was made on each edge and the average weld width in conjunction with the measured weld length was used to calculate the shear area. Shear tension tests were performed in accordance with ASTM Specification D1002-72. The samples were shimmed during testing to prevent an off-set of the grips. The shear test was performed on a 30,000 lb. Instron tensile test machine using a cross-head speed of 0.05 in. per minute (1.3 mm/min.). A minimum period of 220 hours elapsed between welding and testing to ensure sufficient precipitation in the fusion zone had occurred. Results of shear tension tests on the lap-welds are shown in Table XI and Table XII for both alloy combinations. Radiographic analysis was performed at NASA Langely Research Center on the shear tension test specimens after testing. The broken tensile shear test specimens were overlapped with the remaining skin-sheet during radiography to obtain weld soundness associated with the interface and the partial penetration weld of the skin-sheet. Contact prints of the radiographs representing the 0.050 in. (1.3 mm) thick 8090-T6 to 0.120 in. (3.0 mm) thick 2090-T83 weld produced from material that had been chemically milled 0.001, 0.005, and 0.010 in. (0.02, 0.13, and 0.25 mm) are shown in Figures 12 through 14, respectively. The contact prints of the radiographs representing the 0.068 in. (1.3 mm) thick 2095-T6 to 0.120 in. (3.0 mm) thick 2095-T8 welds produced from material that had been chemically milled 0.001, 0.005, and 0.010 in. (0.02, 0.13, and 0.25 mm) are shown in Figures 15 through 17, respectively.

2.3.2 Metallurgical Characterization

Limited metallurgical characterization was also conducted on weld specimens obtained for strength determinations across the partial penetration welds. Optical microscopy was used to determine the depth of penetration associated with the partial penetration welds. Cross-sections of the welds, adjacent to the mechanical property specimens, were removed and prepared for macrographic analysis. This involved grinding to 600 grit silicon-carbide paper and polishing it with 0.05 μm alumina powder suspended in water. Etching was performed by immersion in Keller's Reagent. Photomacrographs of the 0.050 in. (1.3 mm) thick 8090-T6 to 0.120 in. (3.0 mm) thick 2090-T83 welds and 0.050 in. (1.3 mm) thick 2095-T6 to 0.120 (3.0 mm) thick 2095-T8 welds are shown in Figure 18. Microhardness measurements across the welds in the 0.120 in. (3.0 mm) thick 2090-T83 and 2095-T8 material welded under similar condition were performed at 4, 24, 72, and 220 hours after welding. These measurements would be used to determine the degree of degradation in the heat affected zone and the ability of the base metal and weld to precipitation strengthen (naturally age) after welding. Microhardness profiles across the partial penetration welds of the 0.120 in. (3.0 mm) thick 2090-T83 and 0.120 in. (3.0 mm) thick 2095-T8 are shown in Figure 19 and Figure 20, respectively. Fracture surfaces of the returned tensile test specimens were also examined by scanning electron microscopy and the interface area of the returned tension shear test specimens were visually examined for the presence of weld porosity.

2.4 Fabrication of Prototype Panels

Prototype panels were produced by autogenously laser beam welding 3.0 in. (7.6 cm) wide by 1.15 in (2.9 cm) high by 22.5 in. (57.2 cm) long stepped-hat stiffeners to 5.0 in. (12.7 cm) wide by 24 in. (61 cm) long sheet specimens. The stepped-hat stiffeners were superplastically formed at NASA Langley Research from 0.090 in. (2.3 mm) thick 8090-T6 and 2095-T6 material. The skin-sheet represented 0.120 in. (3.0 mm) thick 2090-T83 and 2095-T8 material. The thickness and alloy combinations of interest were 0.090 in. (2.3 mm) thick 8090-T6 to 0.120 in. (3.0 mm) thick 2090-T83 and 0.090 in. (2.3 mm) thick 2095-T6 to 0.120 in. (3.0 mm) thick 2095-T8. Because of the drastic reduction in thickness of the stiffeners that would result from chemically milling 0.010 in. (0.25 mm) per side, it was decided by NASA Langley Research to produce the prototype panels from material that was chemically milled 0.001 and 0.005 in. (0.02 and 0.13 mm) per side prior to welding. This would also offer the opportunity to assess the effect of chemical milling on weld porosity and reduction of weld properties. Material representing the stepped-hat stiffeners and skin sheet for both alloy combinations were forwarded to Chemtronics Corporation, El Cajon, CA for chemical milling of 0.001 and 0.005 in. (0.02 and 0.13 mm) per side. Specimens were chemically milled by immersion in a 32 percent NaOH aqueous solution at 210°F (99°C) for 1 to 5 minutes. Thickness measurements were performed on material prior to shipment and after return from Chemtronics Corporation to confirm the amount of material removed by chemical milling. Material that was chemically milled was wrapped in paper and stored at ambient temperature prior to welding.

The chemically milled material was laser beam welded using parameters established during process development. Minor changes in beam power were attempted based on depth of penetration observations from weld cross-sections; however, welds on two of the panels were later observed to exhibit marginal penetration in the face-sheet. Welding parameters and estimated depth of penetration into the skin for

11

the prototype panels are shown in Table XIII. Weld path was programmed by pendant-teaching through the use of an in-line He-Ne laser. The welding path was established to produce the weld as-near to the vertical member of the stiffener as possible; although, the basic fixturing arrangement utilized for the prototypes did not provide maximum accessibility to the edge of the vertical member. After welding, cross-sections at approximately 1 inch (2.5 cm) from the end of the panels were obtained to determine extent of penetration into the face-sheet. Clamping arrangement utilized for producing the panels was modified to accommodate the larger size of the prototypes. Hand-clamps and 0.375 in. (9.5 mm) thick by 1.0 in. (2.5 cm) wide by 20 in. (51 cm) long steel bars were used to provide clamping force between the stiffener flange and the face-sheet. An auxiliary 0.375 in. (9.5 mm) thick by 1.0 in. (2.5 cm) wide by 20 (51 cm) in. long steel bar was positioned at the top of the stiffener and used to provide additional clamping force between the stiffener and skin-sheet. The clamping arrangement utilized during welding of the prototypes is shown in Figure 21. Note that the auxiliary bar along the top of the stiffeners are not shown in the photographs of Figure 21 for clarity. Because of reduced accessibility for welding of the prototype, the shielding gas arrangement was also modified. This required the use of a 0.250 in. (6.4 mm) inside diameter copper nozzle to be positioned at a 35° angle from the vertical, opposite the welding direction and directed at the leading edge of the weld. A stand-off distance of 0.250 in. (6.4 mm) in front and 0.250 in. (6.4 mm) ahead of the focused beam was maintained. Helium shielding gas was supplied at a flow rate of 200 CFH (94.4 l/min.). Figure 22 are photographs of a completed prototype panel and Figure 23 contains macrographs of the panel cross-section for both alloy combinations that had been chemically milled 0.005 in. (1.3 mm) per side prior to welding. Radiographic analysis of the completed panels were performed at NASA Langely Research Center. Contact prints of the radiographs that had been reduced by a factor of approximately three for each panel condition are shown in Figures 24 through 27.

3.0 DISCUSSION OF RESULTS

3.1 Process Parameters

Process parameter were identified to attain good penetration into the skin and positive weld bead reinforcement at processing speeds offering potentially high productivity; however, concurrent changes in material thicknesses and surface conditions hindered establishment of definitive laser beam welding parameters. Adequate penetration was easily achieved when autogenously welding the various thicknesses of 8090-T6 to 2090-T83 at a beam power of 5.2 to 5.8 kW and travel speeds of 160 IPM (6.8 cm/s). Adequate penetration was also readily accomplished when autogenously welding the various thicknesses of 2095-T6 to 2095-T8 with between 6.0 and 6.7 kW of beam power and travel speeds of 150 IPM (6.4 cm/s). These parameters were identified during the early stages of process development and typically resulted in the weld crown exhibiting positive reinforcement without the addition of filler material. Although these parameters attained the necessary requirements established for the program, it is believed that higher welding speeds, approaching 200 IPM (8.5 cm/s), may be possible through the use of greater beam power and filler metal additions. Processing speeds demonstrated during this program would directly effect the efficiency of producing large panels, having multiple stiffeners, and requiring extensive welding.

As indicated by the range of processing parameters discussed above, lower power levels and higher travel speeds were initially utilized to achieve comparable penetration when welding the alloy combination of 8090-T6/2090-T83 when compared to 2095-T6/ 2095-T8. This was necessary for welding material that was pretreated by wire brushing or mild chemical milling in NaOH to remove 0.001 in. (0.02 mm) per side. It was initially speculated that the higher level of copper contained in alloy 2095 either increased its thermal diffusivity or caused fluid flow conditions that reduced penetration; however, observations of welds on material that was chemically milled to remove 0.005 and 0.010 in. (0.13 and 0.25 mm) per side suggests the difference in penetration may be attributed to the differences in mill-finish. Welds of 2095-T6 to 2095-T8 material that had been aggressively chemically milled tended to have deeper penetration at the higher power levels and slower travel speeds as compared to the 8090-T6 to 2090-T83 that had been chemically milled. As mentioned earlier, concurrent changes in material thicknesses and pretreating conditions precluded the establishment of definitive welding parameters to achieve constant penetration for both alloy combinations. However, based on observations of welds from material that had been chemically milled 0.005 and 0.010 in. (0.13 and 0.25 mm) per side, the difference in heat input required to achieve constant penetration for both alloy combinations may be less than what was initially believed.

Clamping of the top-sheet or stiffener to the face-sheet was found to be critical in achieving good weld quality. The arrangement shown in Figure 7 allowed adequate clamping force along the length of the sheet used for process development and production of mechanical property test specimens. These panels, which involve complete overlap of two 4 in. (10.2 cm) wide by 6.0 in. (15.2 cm) long sheets, presented little difficulty for obtaining adequate clamping force between the top and bottom sheets. This resulted in consistent weld bead uniformity having positive reinforcement for the vast majority of these specimens. However, it was readily observed that the configuration of the prototype panels consisting of a SPF stepped-hat stiffener to the skin presented greater difficulty for achieving adequate clamping force. The clamping arrangement utilized for the prototype panels and shown in Figure 21 did not provide consistent clamping force along the length of the stiffener flange. The resultant welds of the prototype panels exhibited intermittent burn-through along the weld in the stiffener flange and is believed due to insufficient clamping force at those points. The limited scope of this program did not enable the development of a clamping fixture for the prototype panels. However, it is believed that utilization of a fixturing arrangement designed to provide sufficient force between the stiffener flange and skin would provide repeatable weld bead quality similar to that exhibited by the mechanical property specimens.

3.2 Chemical Cleaning

Various cleaning treatments were evaluated for minimizing porosity during laser beam welding of these alloys. These included:

1)   mechanically wire brushing followed by acetone cleaning prior to welding (performed at ARL Penn State),

2)   chemical milling using a 8% NaOH solution at 170°F (77°C) for 60 min. to remove 0.001 in. (0.02 mm) per side (performed at ARL Penn State),

3)   chemically milling using a 20% NaOH solution at 81°F (27°C) for 45 min. to remove 0.001 in. (0.02 mm) per side (performed at Chem-Tron Company, Danbury CT),

4)   chemically milling using a 32 percent NaOH solution at 210°F (99°C) for 5 min. to remove 0.005 in. (0.13 mm) per side (performed at Chemtronics Corporation, El Cajon, CA), and

5)   chemical milling using a 32 percent NaOH solution at 210°F (99°C) for 10 min. to remove 0.010 in. (0.25 mm) per side (performed at Chemtronics Corporation, El Cajon, CA).

Laser beam welds produced on lap configurations for material that was pretreated using the first four cleaning techniques exhibited large amounts of porosity. Metallographic analysis of numerous longitudinal and transverse specimens removed from these welds had shown the vast majority of the pores to be spherical with a shiny internal surface and approximately 0.005 to 0.030 in. (0.12 to 0.76 mm) in diameter. The inability to produce porosity-free welds was also confirmed during analysis of the factorial experiment conducted during process development on material treated by the first two methods. Multiple regression analysis, at a 90 percent probability, showed that alloy combination had a major impact on medium, large, and total porosity found in the laser welds. The analysis indicated that the alloy combination of 8090-T6 to 2090-T83 produced less porosity than the 2095-T6 to 2095-T8 combination. Laser beam welds produced with material pretreated by the fifth cleaning treatment showed minimal porosity based on metallographic analysis. These characteristics led to the belief that the porosity was due to entrapped hydrogen.

In conventional welding of aluminum it is generally agreed that weld porosity is due to hydrogen gas being entrapped during solidification (Refs. 15). It has also been determined that a systems analysis may be used to describe and control the amount of porosity in aluminum arc welds based on available hydrogen sources (Ref. 16). This analysis has been extensively applied to various systems and typically results in a primary source of hydrogen being responsible for weld porosity. Examples are the surface of filler wire for gas metal arc welding of conventional wrought products and internal hydrogen for powder metallurgy alloys and castings. This model for porosity is based on a relatively stable weld pool that is governed by the extent of hydrogen absorbed from available sources and its ability to expel hydrogen pores prior to solidification. However, when a focused, high power laser beam is utilized for welding, the material under the beam evaporates and forms a cavity referred to as a keyhole. As the heat source moves along the base material the keyhole continually melts material at the front edge with solidification occurring at the rear. The keyhole is maintained by balancing the hydrodynamic forces of the pool with the vapor pressure within the cavity. Although a complete treatise does not exist, results of prior investigations have indicated that vaporization of volatile alloying elements, such as magnesium and lithium, and keyhole instability may also be responsible for porosity during laser beam welding of aluminum (Refs. 17 and 18).

Thermally induced oxidation during primary processing of aluminum-lithium alloys results in surface reactions between metal and water vapor or H_2. The reaction product, atomic hydrogen, is available for dissolution into the metal (Ref. 19). This results in increasing concentrations of hydrogen near the metal surface until the maximum mutual solubility of H and Li is exceeded, and LiH is precipitated at grain boundaries (Refs. 20-23). Lithium is also consumed in the near-surface metal creating a lithium depleted zone in conjunction with the formation of an atomic hydrogen and/or LiH enriched zone (Ref. 24). The lithium depleted zone has been reported to be approximately 0.004 in. (100 μm) for alloy 8090; however, since the process is diffusion controlled the width of the lithium depleted zone would be dependent on the thermal treatments used during processing, such as solution heat treatment (Ref. 25).

14

Various prior investigators have shown strong cause-and-effect relationships between the zone of atomic hydrogen and/or LiH enrichment inherent in aluminum-lithium alloys and weld porosity. The earliest indications of propensity for weld porosity for aluminum-lithium alloys was reported on the Soviet alloy 01420 (Al-5.0Mg-2.2Li) which was reviewed by Pickens (Ref. 26). Pickens reported that many of the Soviet welding investigations determined the reason for high weld porosity associated with alloy 01420 is the surface reactivity with ambient moisture, making pre-welding surface preparation critically important (Refs. 27-30). Similar results have been reported in the United States for alloys 2090 and 2095. Martukanitz, et al., found during gas tungsten arc welding evaluations on 2090 alloy that porosity increased as the thickness of the material decreased which he attributed to a hydrogen-enriched layer near the surface (Ref. 31). He also found that the amount of porosity of butt welds in 0.063 in. (1.6 mm) thick 2090 decreased as the amount of surface was removed by both chemical milling with NaOH and dry machining. Using reduction in joint strength and radiographic analysis as criteria, Martukanitz, et al., recommended removing 0.010 in. (0.25 mm) from each side when welding 0.063 in. (1.6 mm) thick material and 0.004 in. (0.1 mm) from each side when welding thicknesses approaching 0.126 in. (3.2 mm). Kerr and Merino found that dry mechanical milling to remove 0.010 in. (0.25 mm) per side on 0.126 in. and 0.248 in. (3.2 mm and 6.3 mm) thick 2090 resulted in variable polarity plasma arc welds that were radiographically acceptable (Ref. 32). They also found that the effectiveness of the cleaning process was maintained for welds produced within 10 days of cleaning. Results of welding investigations for alloy 2095 indicate that a standard chemical milling treatment, 30% NaOH aqueous solution at 212°F (100°C) to remove the surface layer, may be used to produce porosity-free welds by the gas tungsten arc welding process (Ref. 33). These earlier findings strongly support the contention that the primary source of porosity formed at the interface during laser beam welding of these aluminum-lithium alloys was the hydrogen-enriched region near the surface of the material. Removing this region by chemical milling 0.010 in. (0.25 mm) per side eliminated the primary source of hydrogen, and reduced the porosity found at the interface.

It was also observed by metallographic analysis during this investigation that lap welds produced by laser beam welding of the alloy combination of 2095/2095 exhibit a greater number of pores at the interface than the combination of 8090/2090 when insufficient pretreatments were used, such as with the first four cleaning techniques described above. However, results of subsequent evaluations utilizing chemical milling of 0.010 in. (0.25 mm) per side indicated that the difference in weld porosity at the interface between the two alloy combinations was greatly reduced when sufficient material was removed prior to welding. This is illustrated in Figure 8 which shows the reduction of porosity at the interface for both alloy combinations when 0.010 in. (0.25 mm) per side was removed by chemical milling prior to welding. Since surface enrichment of hydrogen is through diffusion it may be effected by both time and temperature during elevated processing, such as solution heat-treating. Higher processing temperatures at longer times would result in a thicker surface layer being enriched in hydrogen. A possible explanation for the greater amount of porosity at the interface associated with the 2095-T6 welded to 2095-T8 specimens may be the thermal processing used to produce the material.

The results of radiographic analysis of shear tension test specimens and prototype panels showed linear porosity at the root of all of the laser beam welds. Radiographic analysis of the fractured shear tension test specimens indicated that although porosity at the interface of the stiffener and skin was dramatically reduced by chemical milling 0.010 in. (0.25 mm) per side prior to welding, linear porosity continued to be exhibited in the root of the weld. This is illustrated in Figures 12 through 17, which represent photographs of radiographs for the fractured shear tension test specimens of both alloy combinations that were chemically milled 0.001, 0.005, and 0.010 in. (0.02, 0.13, and 0.25 mm) prior to welding. The radiographic image to the right in the photographs represent the weld through the stiffener-sheet, and the image on the left is of the partial penetration of the skin. As seen in the photographs, chemical milling of 0.005 in (0.13 mm)

for the 8090/2090 combinations and 0.010 in (0.25 mm) for the 2095/2095 greatly reduced porosity at the interface (images on the right). However, gross, linear porosity was evident in the root of the welds (images to the left) regardless of alloy combination or amount that had been chemically milled prior to welding. It appears that the linear porosity associated with the weld-root in the skin is process related. The dark coloration and non-symmetrical shaped exhibited by some of these pores during subsequent metallographic analysis suggest that the linear porosity may be due to vaporization of low-vapor point constituents such as lithium, which may lead to keyhole instability. Further investigations would be required to determine the relationship between the primary process variables and the linear porosity found in the weld-roots.

3.3 Mechanical Properties

The results of tensile tests performed on the 0.120 in. (3.0 mm) thick 2090-T83 and 2095-T8 face-sheet having partial penetration welds are shown in Table VIII and Table IX for both alloys. Also included in the Tables are tensile test results for unwelded base metal. The mean of five samples for ultimate tensile strength across the partial penetration welds of 2090-T83 was 61.6 KSI (425 MPa) as compared to the average base metal strength of 80.4 KSI (555 MPa) for 2090-T83. The mean of five samples representing partial penetration in the 2095-T8 was 58.8 KSI (406 MPa) and exhibited an average base metal strength of 89.9 KSI (620 MPa). The standard deviation around the mean values of ultimate tensile strength across the partial penetration welds for both alloys were approximately 3 KSI (23 MPa). The percent elongation, in 1.0 in. (2.54 cm) gage length, measured across the partial penetration welds were significantly less than the unwelded base metal. The mean elongation for the welds on 2095-T8 material was 0.8 percent and no appreciable elongation was observed for the partial penetration welds on 2090-T8 material. In all cases for the 2090-T83, and one case for the 2095-T8, yield strength was not obtained due to failure occurring prior to reaching the 0.2 percent off-set. All failures occurred at the interface between the fusion zone of the partial penetration weld and the heat affected zone and is representative of these alloys. The low elongation measured in these samples is not surprising, since aluminum alloys containing high levels of copper typically exhibit low elongations across the weld. Also, the percent elongation measured from tensile tests is not always a good indication of joint ductility.

The values for ultimate tensile strength discussed above represent a joint efficiency of 77 percent for 2090-T83 and 65 percent for 2095-T8 for the partial penetration welds; however, comparison of joint efficiencies should not be made between the two alloys based on these values. The strength across the partial penetration welds of the 2090-T83 represented penetration of 40 percent of the thickness; whereas, the partial penetration of the 2095-T8 exhibited 60 percent penetration. This is illustrated in the photomacrographs of the lap-welds prior to removal of the top-sheet in Figure 18. The deeper penetration associated with the 2095-T8 would be indicative of higher thermal profiles in the heat affected zone and greater degradation of properties in this region. Because of this, a valid comparison of joint efficiencies associated with the partial penetration welds of both alloys could not be made.

Results of shear tension tests to measure shear strength at the interface for lap-welds of both alloys combinations are shown in Tables XI and XII for samples retained by ARL Penn State. As mentioned earlier, alloy combinations of 8090-T6 to 2090-T83 and 2095-T6 to 2095-T8 in two face-sheet thicknesses were produced from material that had been chemically milled 0.001, 0.005, and 0.010 in. (0.02, 0.13, 0.25 mm) prior to welding. The test results shown in tables XI and XII represent the 0.050 in. (1.3 mm) thick 8090-T6 to 0.120 in. (3.0 mm) thick 2090-T83 and 0.068 in. (1.7 mm) thick 2095-T6 to 0.120 in. (3.0 mm) thick 2095-

16

T8 specimens retained by ARL Penn State. The 0.050 in. 91.3 mm) thick 8090-T6 to 0.095 in. (2.4 mm) thick 2090-T83 and 0.068 in. (1.7 mm) thick 2095-T6 to 0.095 in. (2.4 mm) thick 2095-T8 specimens were forwarded to NASA Langley Research Center for tension shear tests.

The results indicate appreciably higher weld shear strengths are achieved with the 2095-T6 to 2095-T8 alloy combination when compared to 8090-T6 to 2090-T83. Regression analysis at a 90 percent probability showed no discernible differences in shear strength of the lap-welds that could be attributed to the amount of material removed by chemical milling for either alloy combination. Therefore, the shear strength values for all samples representing each alloy combination were grouped for comparison. The mean value, representing nine samples, for shear strength of the 0.050 in. (1.3 mm) thick 8090-T6 to 0.120 in. (3.0 mm) thick 2090-T83 was 11.7 KSI (81 MPa) with a standard deviation of 1.1 KSI (8 MPa). The mean shear strength for nine samples of 0.068 in. (1.7 mm) thick 2095-T6 to 0.120 in. (3.0 mm) thick 2095-T8 was 18.8 KSI (130 MPa) with a standard deviation of 2.4 KSI (17 MPa). The mean shear strength of 18.8 KSI (130 MPa) for the 2095-T6 to 2095-T8 alloy combination is comparable to the minimum shear strength of 16 KSI (110 MPa) reported for aluminum alloy 2319 (Ref. 30). The high shear strength displayed by the 2095-T6/2095-T8 combination is believed to be attributed to the ability of the alloy to precipitation strengthen after welding.

3.4 Weld Characterization

The hardness measurements across the partial penetration welds at various times after welding for 2090-T83 and 2095-T8 are shown in Figure 13 and Figure 14, respectively. It appears from the profiles that a minor increase in hardness occurs after welding the 2090-T83 alloy; however, the increase in hardness after welding of 2095-T8 is appreciable. The fusion zone of the 2095-T8 had increased from approximately 75 VHN to 100 VHN within 220 hours after welding. A similar increase was found in the heat affected zone of alloy 2095-T8 after 220 hours. This is due to the ability of 2095-T8 to precipitation strengthen, or naturally age, after welding. Within the fusion zone and at positions in the heat affected zone experiencing high elevated temperatures, strengthening precipitate undergo dissolution. Upon cooling, strengthening particles will continue to precipitate within the matrix and the degree of strengthening will be primarily governed by the kinetics of the precipitation reaction. The ability of alloy 2095-T8 to naturally age after welding is greatly responsible for the increased weld shear strength exhibited by this alloy. This phenomena should also result in higher strength across the partial penetration welds of 2095-T8 when compared to 2090-T83; however, because of unequal penetration between the two alloys evaluated, this was not confirmed.

Analysis of fracture surfaces of the samples used to measure strength across the partial penetration of the face-sheet and weld shear strength of the interface was conducted. Scanning electron microscopy was utilized to examine the fracture surfaces of the partial penetration welds that were tensile tested. The scanning electron microscope images of the fusion zone appeared similar for 2090-T83 and 2095-T8; however, the appearance of the fracture surface encompassing the heat affected zone beneath the partial penetration varied between the alloys. Representative scanning electron photomicrographs are shown in Figure 18 and Figure 19 for 2090-T83 and 2095-T8, respectively. The heat affected zone, shown below the fusion zone in the figures, tended to exhibit a striated structure for 2090-T8; whereas, the heat affected zone for the 2095-T8 displayed a granular appearance with some evidence of striations near the fusion zone interface. Microporosity was present in the partial penetration welds representing both alloys.

17

Visual examination of the fracture surfaces of the samples used to determine weld shear strength was used to ascertain the effectiveness of chemical milling 0.001, 0.005, 0.010 in. (0.02, 0.13, and 0.25 mm) for eliminating porosity. This examination indicated that weld porosity at the interface was virtually eliminated for all degrees of chemical milling of welds representing 8090-T8 to 2090-T83. One pore, greater approximately 0.020 in. (0.51 mm) in diameter, was found in each group of 8090-T6 to 2090-T83 samples that had been chemical milled 0.001, 0.005, and 0.010 in. (0.02, 0.13, and 0.25 mm) per side. All other samples of 8090-T6 to 2090-T83 showed no porosity. Conversely, the 2095-T6 to 2095-T8 welds exhibited an average of 3 pores at the interface, approximately 0.020 in. (0.51 mm) in diameter, per sample when chemically milled to remove 0.001 and 0.005 in. (0.02 and 0.13 mm) per side. The number of pores at the fracture surface of the 2095-T6 to 2095-T8 was seen to decrease when chemically milled to remove 0.010 in. (0.25 mm) per side to an average of one pore per sample. The level of porosity associated with the fracture surfaces of the 2095-T6 to 2095-T8 tension shear test samples did not appear to dramatically effect the shear strength. Multiple regression analysis of shear strength (as the dependent variable) as a function of weld shear area and number of pores (as independent variables) could not establish a strong statistical relationship for the 2095-T6 to 2095-T8 tension shear test samples.

4.0 CONCLUSIONS

An evaluation to determine the feasibility of laser beam welding of aluminum-lithium alloys for cryogenic tankage alloys has been completed. Conclusions based on the results of this evaluation are shown below for the three major categories investigated:

4.1 Laser Beam Welding Process Evaluation

1) Laser beam welding is a feasible joining technique for producing aluminum-lithium built-up structures. Adequate penetration may be produced on the alloys at power levels of 5 to 7 kW and travel speeds of 150 to 160 IPM (6.4 to 6.8 cm/s),

2) The laser beam welding process provided accessibility such that lap-welds may be produced very near the edge of the vertical member on the stepped-hat stiffeners of the prototype panels,

3) The high processing speeds demonstrated during the program may be directly related to high production rates and low cost operations,

4) Adequate clamping force between the stiffener and skin was critical in achieving consistent weld quality along the length of the stiffeners. Adequate clamping force improves the quality of the weld surface but does not eliminate internal porosity.

4.2 Pretreatment and Porosity Evaluation

1) Aggressive pretreatment in the form of alkaline chemical milling was required to reduce porosity at the weld interface (between the stiffener and skin) but does not eliminate porosity associated with the root of the weld.

2) The porosity at the weld interface (between the stiffener and skin) appears to be due to the hydrogen enriched layer associated with these alloys while the porosity at the weld-root appears to be process related.

3) Removing 0.001, 0.005, and 0.010 in. (0.02, 0.13, and 0.25 mm) per side by chemical milling did not appear to affect the overall shear strength of the weld.

4.3 Mechanical Property Characterization

1) Tensile tests of laser beam welds representing partial penetration of the face-sheet provided a joint efficiency of 77 percent (at 40 percent through-thickness penetration) for 2090-T83 and 65 percent (at 60 percent through-thickness penetration) for 2095-T8.

2) The alloy combination of 2095-T6 to 2095-T8 exhibited much higher weld shear strength at the interface when compared to the combination of 8090-T6 to 2090-T83. The average shear strength of welds between 2095-T6 to 2095-T8 was 18.8 KSI (130 MPa) as compared to an average shear strength of 11.7 KSI (81 MPa) for 8090-T6 to 2090-T8 combination,

3) The improved shear strength of the 2095-T6 to 2095-T8 combination is believed to be due to the ability of alloy 2095 to precipitation strengthen or naturally age after welding,

5.0 RECOMMENDATIONS

Based on the results of this initial investigation to determine the feasibility of laser beam welding aluminum-lithium alloys for cryogenic tankage applications, it is recommended that further evaluations be conducted. Laser beam welding has demonstrated the ability of offering high production rates, and possibly lower cost, for joining of stiffeners to face-sheet. Extrinsic process development, such as fixture and joint design, should be optimized for laser beam welding of larger prototype panels. Modification of processing parameters, such as the addition of filler metal and alternate shielding gas arrangements, should be investigated for reducing weld-root porosity.

Direct comparison of laser beam welded and resistance welded structures should then be performed to ascertain structural integrity, quality, and costs associated with these processes. The need to aggressively, chemically pretreat aluminum-lithium alloys for minimizing weld porosity at the interface should also be quantified if they are to be accepted for welded, aerospace applications.

6.0 REFERENCES

1. Proceedings of the Conference on Advanced Aluminum Technology for Cryogenic Tank Applications, NASA Langley Research Center, Hampton, VA, 1987.

2. General Dynamics Space Systems, "Space Transportation Architecture Study," Report GDSS-STAS-87-002, 1987.

3. Tack, W. T. and L. W. Loechel, "Weldalite™ 049: Applicability of a New High Strength, Weldable Al-Li-Cu Alloy," Aluminum-Lithium Alloys, Proceedings of the Fifth International Aluminum-Lithium Conference, Vol. III, Materials and Component Engineering Publication Ltd., Birmingham, UK, 1989, p. 1462.

4. Anton, C. E., Rasmussen, P., Thompson, C., Latham, R., Hamilton, H., Ren, B., Gandhi, C, and Hardwick, D., "Low Cost, SPF Aluminum Cryogenic Tank Structure for ALS," NASA Contractor Report 189654, Under Contract NAS1-18590 to Rockwell International North American Aircraft, NASA Langley Research Center, Hampton VA, 1992.

5. Cross, C. E., Tack, W. T., "Selection and Weldability of Aluminum-Lithium Alloys," Metals Handbook-Vol. 6, ASM International, Materials Park, OH, 1993.

6. W. E. Quist and G. H. Narayanan, "Aluminum-Lithium Alloys," Treatise on Mat. Sci. and Tech., vol. 31, pp. 219-254, 1989.

7. T. J. Langan and J. R. Pickens, "Identification of Strengthening Phases in the Al-Cu-Li Alloy WeldaliteTM 049," Proc. 5th Int. Al-Li Conf., Williamsburg, pp. 691-700, 1989.

8. Martukanitz, R. P., Natalie, C. A., and Knoefel, J. O., "The Weldability of an Al-Cu-Li Alloy," Journal of Metals, Vol. 39 (11), 1987, p. 42.

9. Molian, P. A. and T. S. Srivatsan, "Weldability of Al-Li-Cu Alloy Using Laser Welding," Proceedings of the Fifth International Aluminum-Lithium Conference, Vol. III, Materials and Component Engineering Publication, Ltd., UK 1989, p. 1439.

10. Martukanitz, R. P., Natalie, C. A., and Knoefel, J. O., "The Weldability of 2090 (An Al-Li-Cu Alloy)," Journal of Metals, Vol. 39 (11), 1987, p. 38.

11. Pickens, J. R., "The Weldability of Lithium-Containing Aluminum Alloys," Journal of Material Science, Vol. 20, 1985, p. 4247.

12. Fridlyander, I. N., et al., Translated from Metallovendenie i Termicheskaya Obrabotka Metallov (3), 1975, p.53.

13. Pickens, J. R., "The Weldability of Lithium-Containing Aluminum Alloys," Journal of Material Science, Vol. 20, 1985, p. 4247.

14. Martukanitz, R. P., Natalie, C. A., and Knoefel, J. O., "The Weldability of 2090 (An Al-Li-Cu Alloy)," Journal of Metals, Vol. 39 (11), 1987, p. 38.

15.   Howden, D. G. and Milner, D. R., "Hydrogen Absorption in Arc Welding," <u>British Welding Journal</u>, Vol. 10, 1963, p. 304.

16.   Martukanitz, R. P. and Michnuk, P. R., "Sources of Porosity in Gas Metal Arc Welding of Aluminum," <u>Aluminum</u>, Vol. 58 (5), 1982, p.276.

17.   Marsico, T. A. and Kossowsky, R., "Physical Properties of Laser Welded Aluminum-Lithium Alloy 2090," <u>Proceedings of the Fifth International Aluminum-Lithium Conference</u>, Materials and Components Engineering Publications, Ltd., Birmingham (UK), 1989, p. 1447.

18.   Katayama, S., Ludwin, C. D., Danko, J. C., and McKay, T. D., "Laser Weldability of Aluminum Alloys," <u>Conference Proceedings of Recent Trends in Welding Science and Technology</u>, ASM, 1990, p.687.

19.   Dickenson, R. C., Wefers, K., and Lawless, K. R., "Internal Lithium Hydride Precipitation in Al-Li Alloys," <u>Proceedings of the Fifth International Aluminum-Lithium Conference</u>, Materials and Component Engineering Publications Ltd., Birmingham (UK), 1989, p. 1337.

20.   Dickenson, et al., op cit., p. 1339.

21.   Bavarian, B., Becker, J., Parikh, S. N., and Zamanzadeh, M., "Localized Corrosion of 2090 and 2091 Al-Li Alloys," <u>Proceedings of the Fifth International Aluminum-Lithium Conference</u>, Materials and Component Engineering Publications Ltd., Birmingham (UK), 1989, p. 1231.

22.   Fridlyander, I. N., Metal Oved. Term. Obrab. Met., (4), 1970, p. 44.

23.   Wefers, K and Mozelewski, F. A., "Surface Chemistry of Al-Li-Cu Alloys," <u>Proceedings of the 8th International Light Metals Conference</u>, 1987.

24.   Dickenson, op cit., p. 1339.

25.   Roth, A. and Kaesche, H. "Electrochemical Investigation of Technical Aluminum-Lithium Alloys," <u>Proceedings of the Fifth International Aluminum-Lithium Conference</u>, Materials and Component Engineering Publications Ltd., Birmingham (UK), 1989, p. 1215.

26.   Pickens, J. R., "The Weldability of Lithium-Containing Aluminum Alloys," <u>Journal of Materials Science</u>, Vol. 20, 1985, 4247.

27.   Mironenko, V. N., Evstifeev, V. S., Lubenets, Karshukova, S. A., Zakherov, V. V., and Litvintsev, A. I., <u>Welding Production</u>, English Translation), Vol. 26 (1), 1979, p. 30.

28.   Mironenko, V. N., Evstifeev, V. S., and Korshunkova, S. A., <u>Welding Production</u>, Vol. 24 (12), 1977, p. 44.

29.   Fedoseev, V. A., Ryazansev, V. I., Shiyaesa, N. V., and Arbuzov, Yu. P., ibid., Vol. 12 1979) 19, Translation of Svar. Proizvod. (No. 6, 1978) p. 15.

30.   Kainova, G. E. and Malinkina, T. I., Metal Science of Heat Treating Metall. Oved. Termi. Obrab. Met.) (No. 2 1968) 22, Translation p. 104.

31.   Martukanitz, R. P., Natalie, C. A., and Knoefel, J. O., "The Weldability of 2090 (An Al-Li-Cu Alloy)," Journal of Metals, (11), 1987, p. 38.

32.   Kerr, J. R. and Merino, R. E., "Cryogenic Properties of VPPA Welded Aluminum-Lithium Alloys," Proceedings of the Fifth International Aluminum-Lithium Conference, Materials and Component Engineering Publications Ltd., Birmingham (UK), 1989, p. 1491.

33.   Kramer, L. S. and Pickens, J. R., "Microstructure and Properties of a Welded Al-Cu-Li Alloy," Welding Journal-Research Supplement, Vol. (4), 1992, p. 115-s.

34.   Nelson, F. G. and R. L. Rolf, "Shear Strength of Al Alloy Fillet Welds," Welding Journal-Research Supplement, Vol. 45 (2), 1966, p. 82s.

7.0 FIGURES AND TABLES
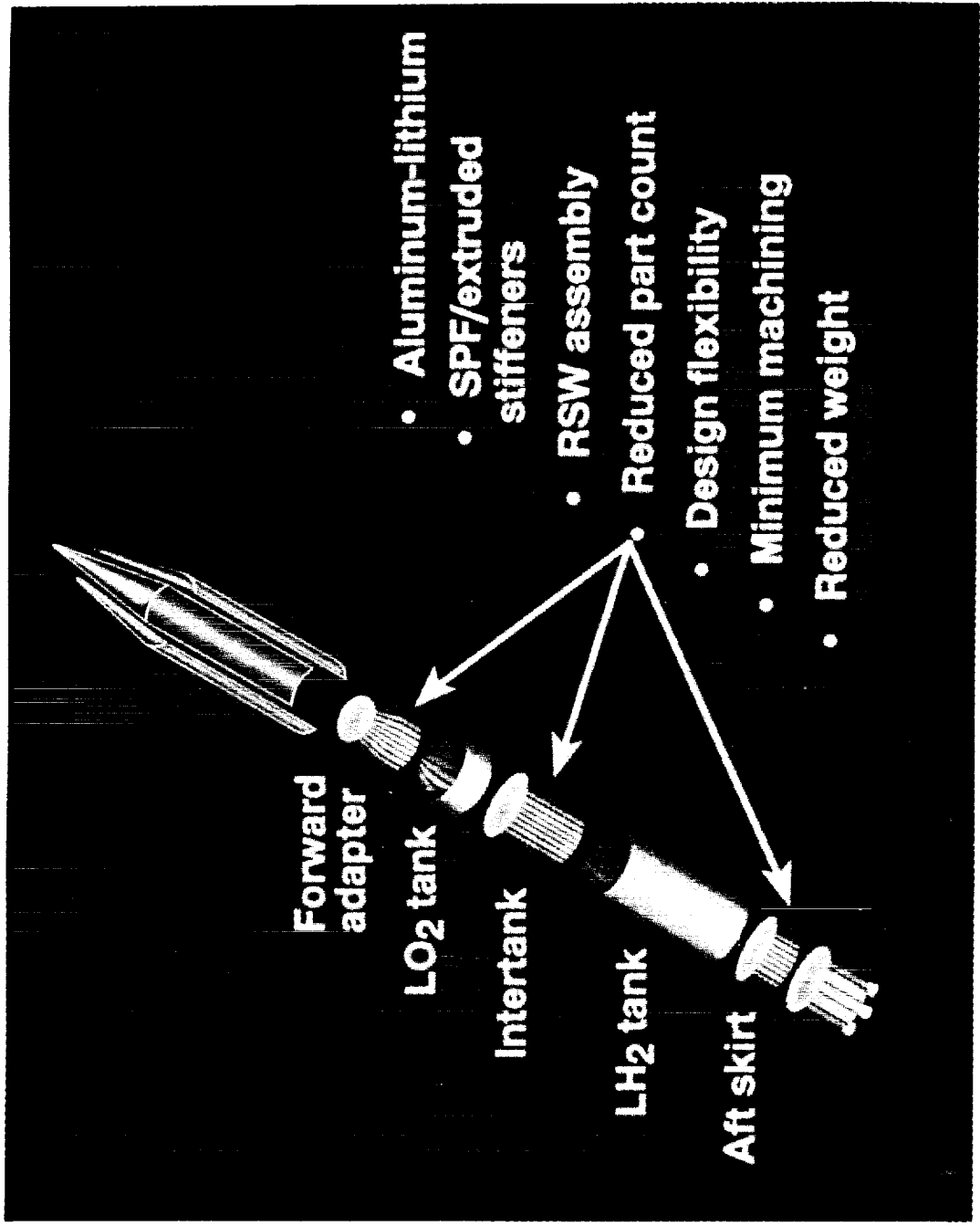
Figure 1: Artist's Rendition of an Advanced Launch Vehicle Showing Liquid Oxygen and Liquid Hydrogen Tanks.

SUPERPLASTICALLY FORMED (SPF) STIFFENERS
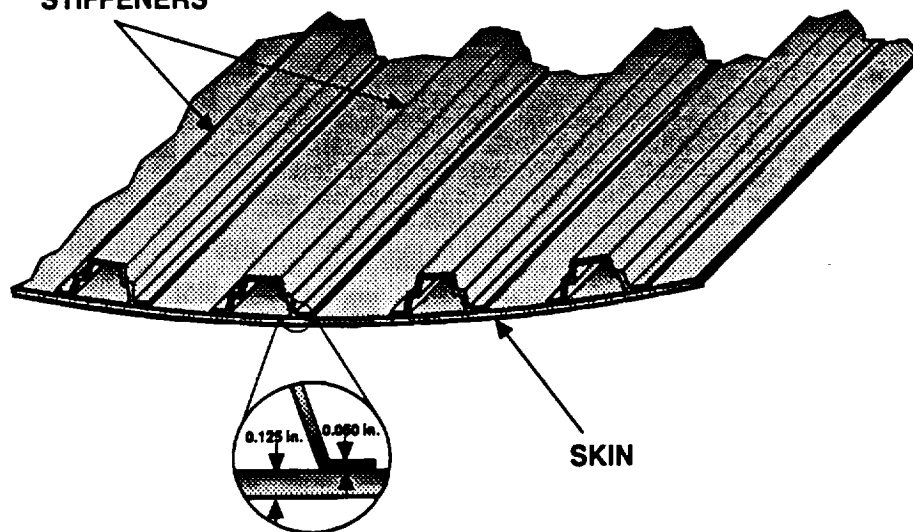
SKIN

0.125 in. 0.060 in.

JOINT DETAILS

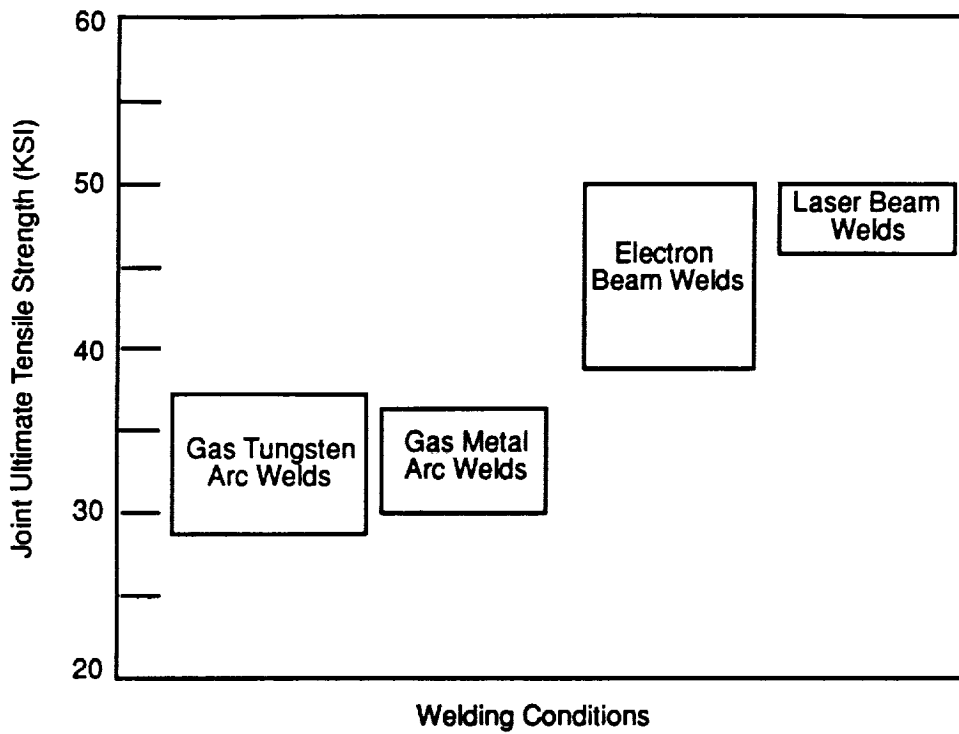**Figure 2:** Cross-section of One Concept That Has Been Proposed for Producing the Built-Up Structure.

Figure 3: A Comparison of Ultimate Tensile Strength of Butt-Welds in Alloy 2090-T83 Produced Using Various Welding Processes (Refs. 8 and 9).
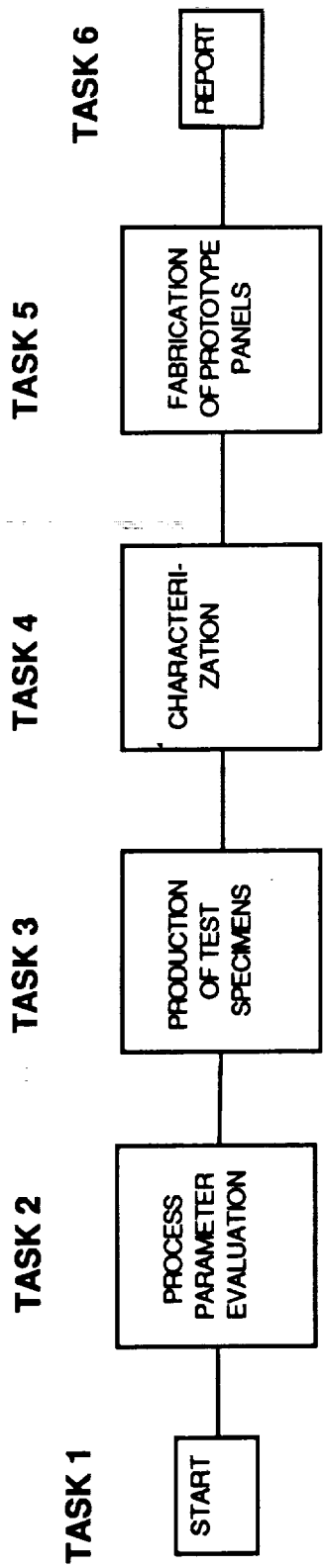
Figure 4: Diagram Showing Task Sequences for Program to Determine Feasibility of Laser Beam Welding Aluminum-Lithium Alloys for Cryogenic Tank Applications.

TROUGH

M5

FLEX-COVER

Z AXIS

BEAM

V AXIS

SUPPORTS

PITCH AXIS

YAW AXIS

X AXIS
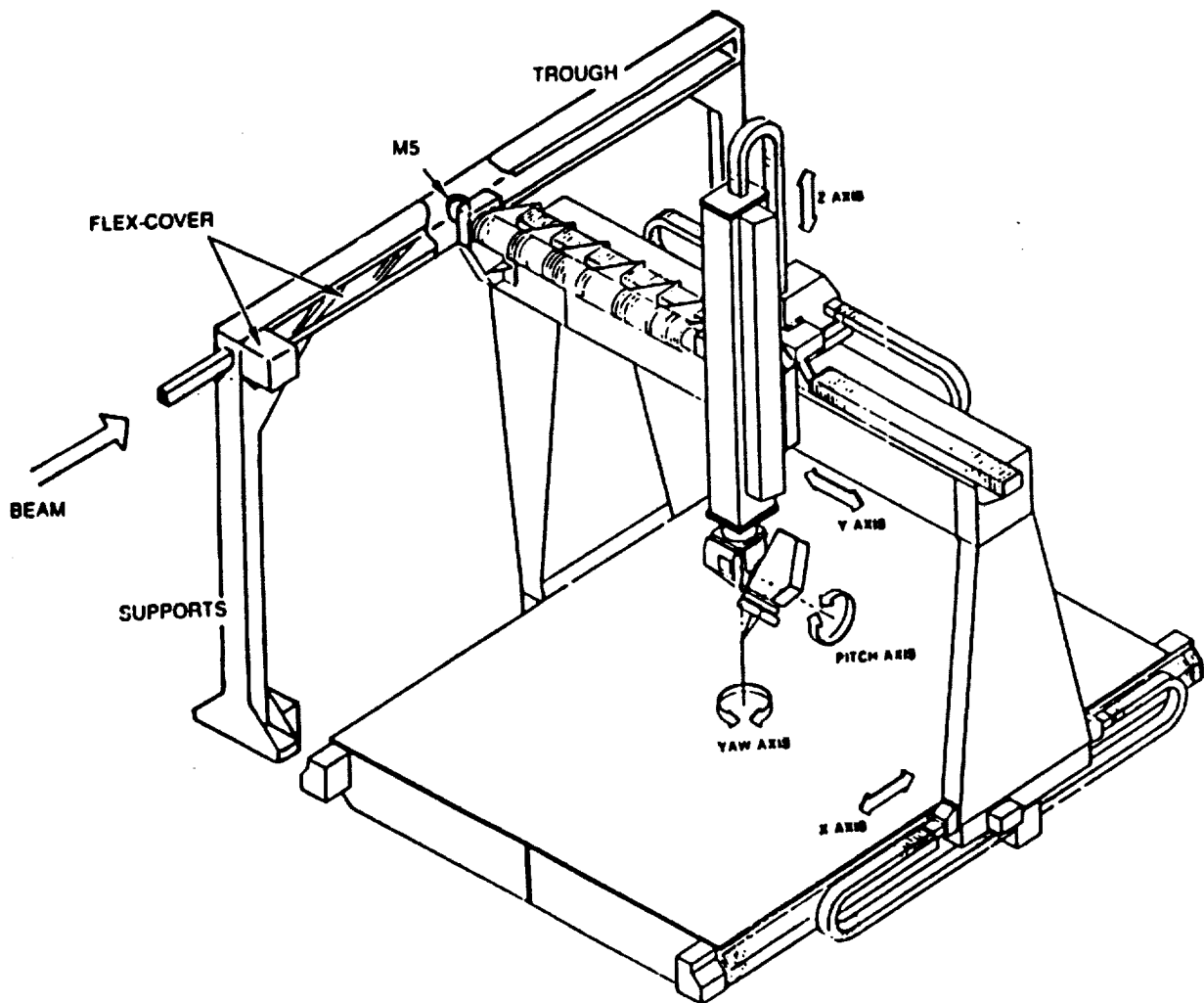
Figure 5:   Schematic of Laser Articulating Robotic System (LARS) Used for Laser Beam Welding Program.
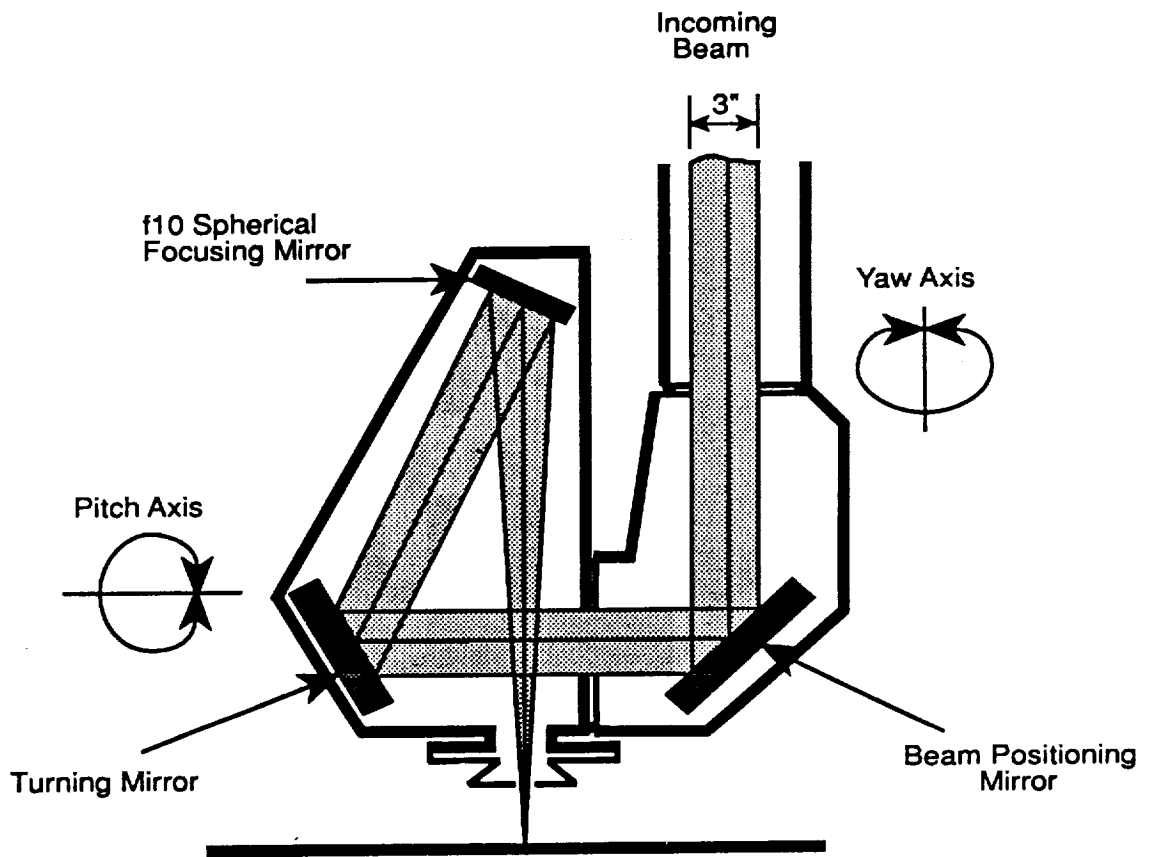
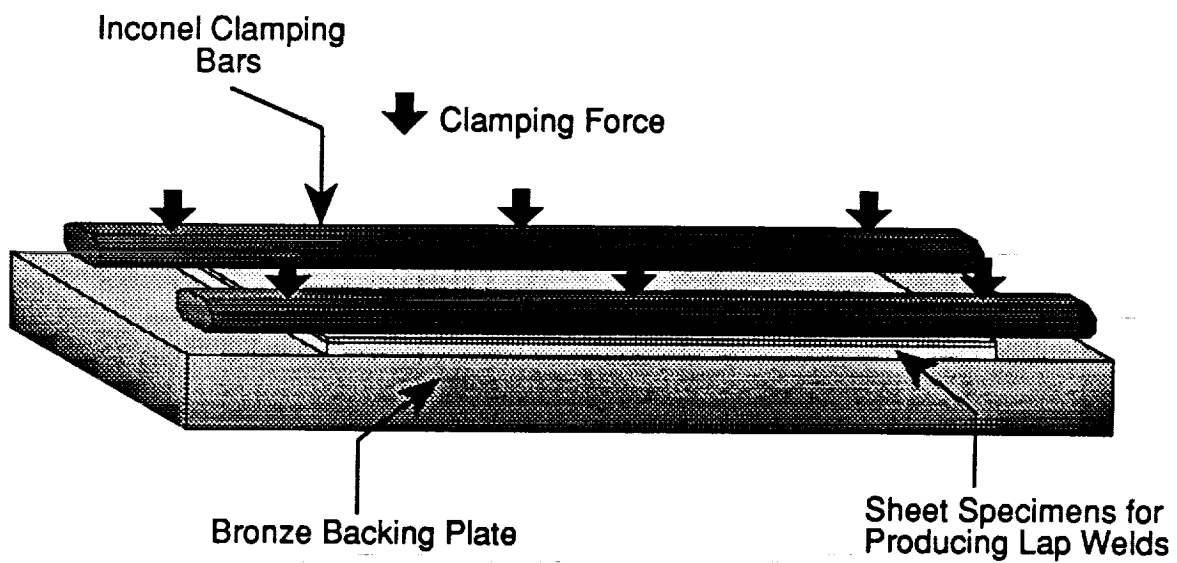Figure 6: Optical Arrangement Used for the Laser Articulating Robotic
System (LARS).

Figure 7: Clamping Arrangement Utilized for Initial Process Parameter
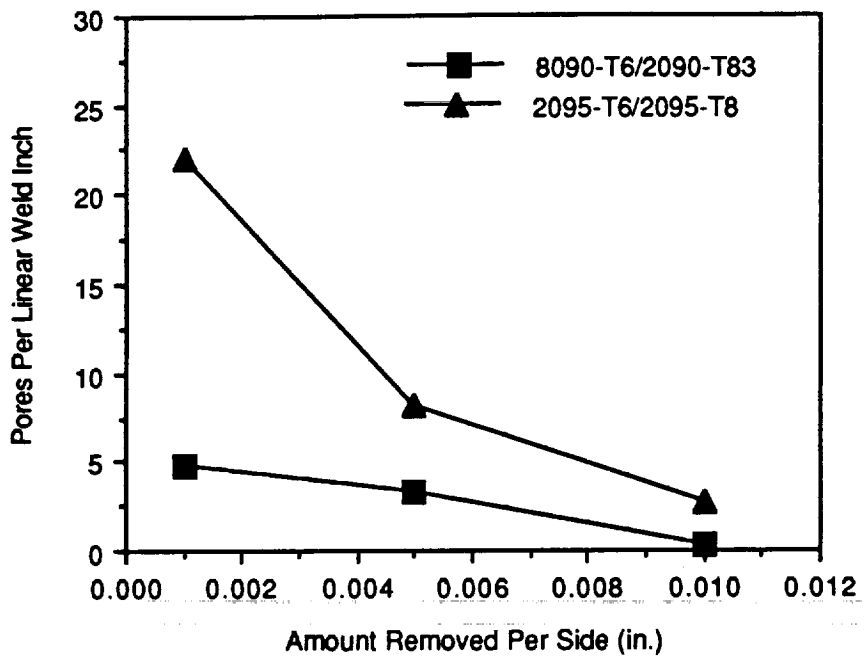Development for Lap-Welds.

Figure 8: Amount of Porosity Associated With the Interface of Laser Beam Welded Samples that had been Chemically Milled Various Amounts Prior to Welding.
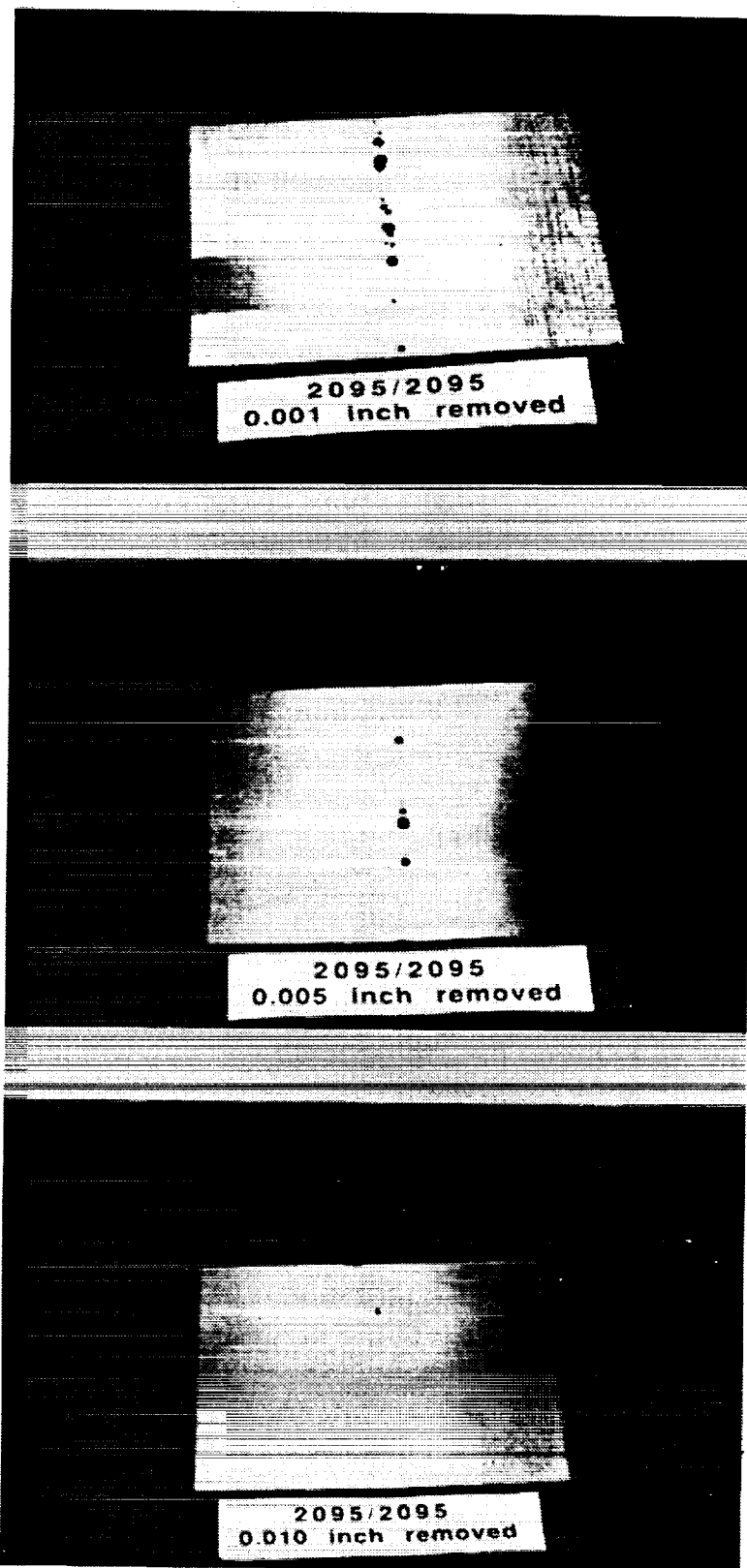
Figure 9: Photographs of 2095-T6 to 2095-T8 Laser Beam Weld Specimens
After Dye Penetrant Testing Showing Degree of Porosity at the
Interface Associated With Chemical Milling of 0.001, 0.005,
and 0.010 Inch (0.02, 0.13, and 0.25 mm) Per Side.

Figure 10: Photographs of 8090-T6 to 2090-T83 Laser Beam Weld Specimens After Dye Penetrant Testing Showing Degree of Porosity at the Interface Associated With Chemical Milling of 0.001, 0.005, and 0.010 Inch (0.02, 0.13, and 0.25 mm) Per Side.
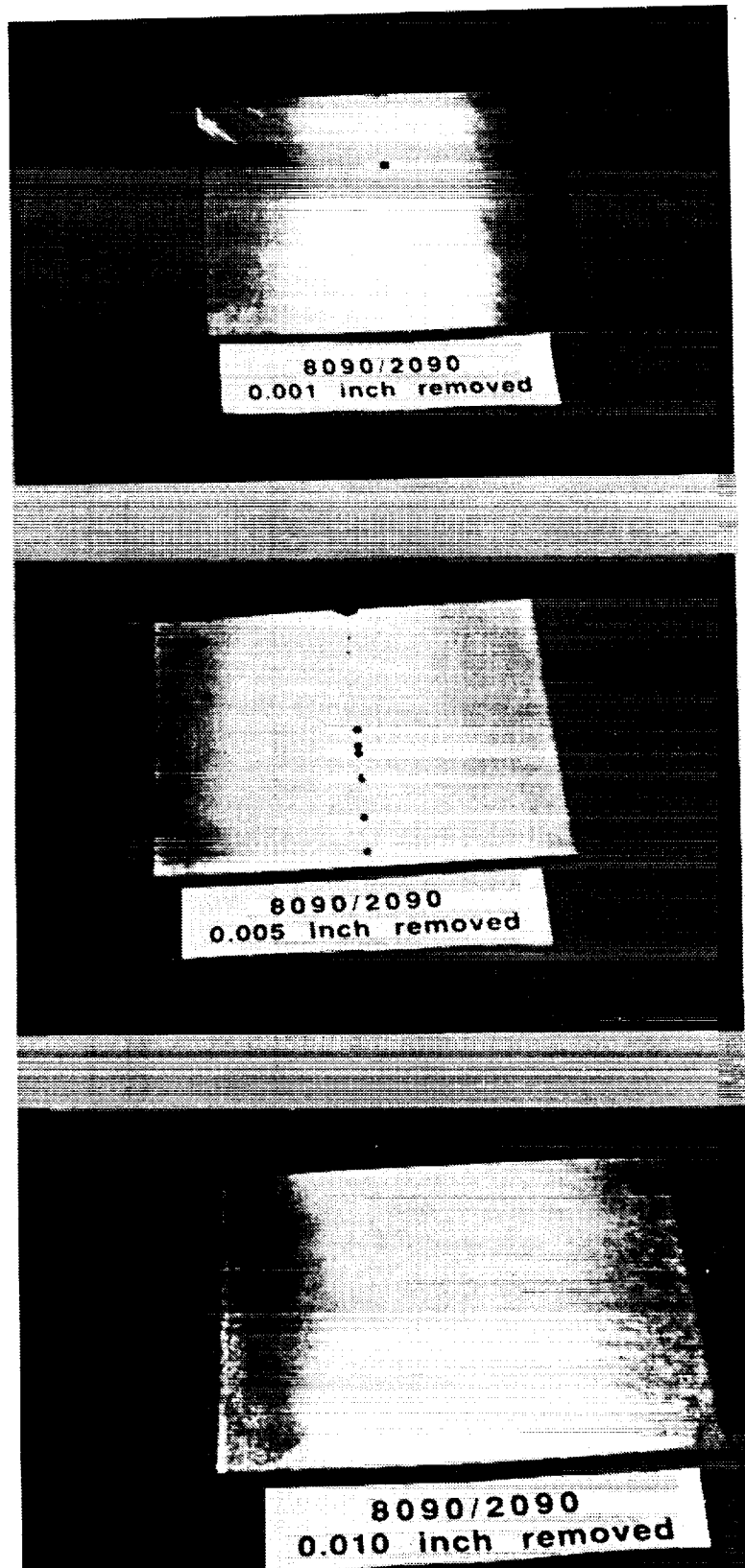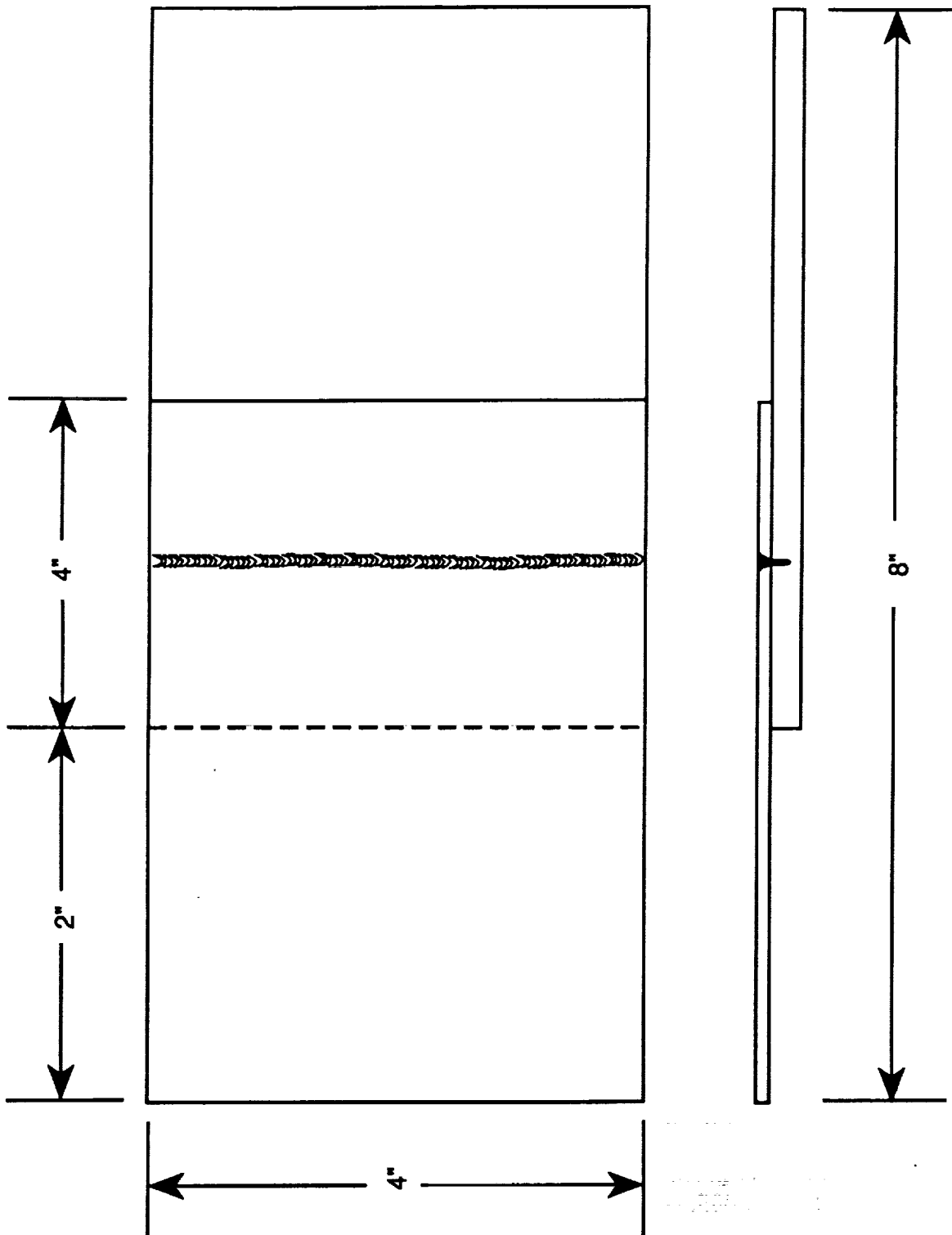
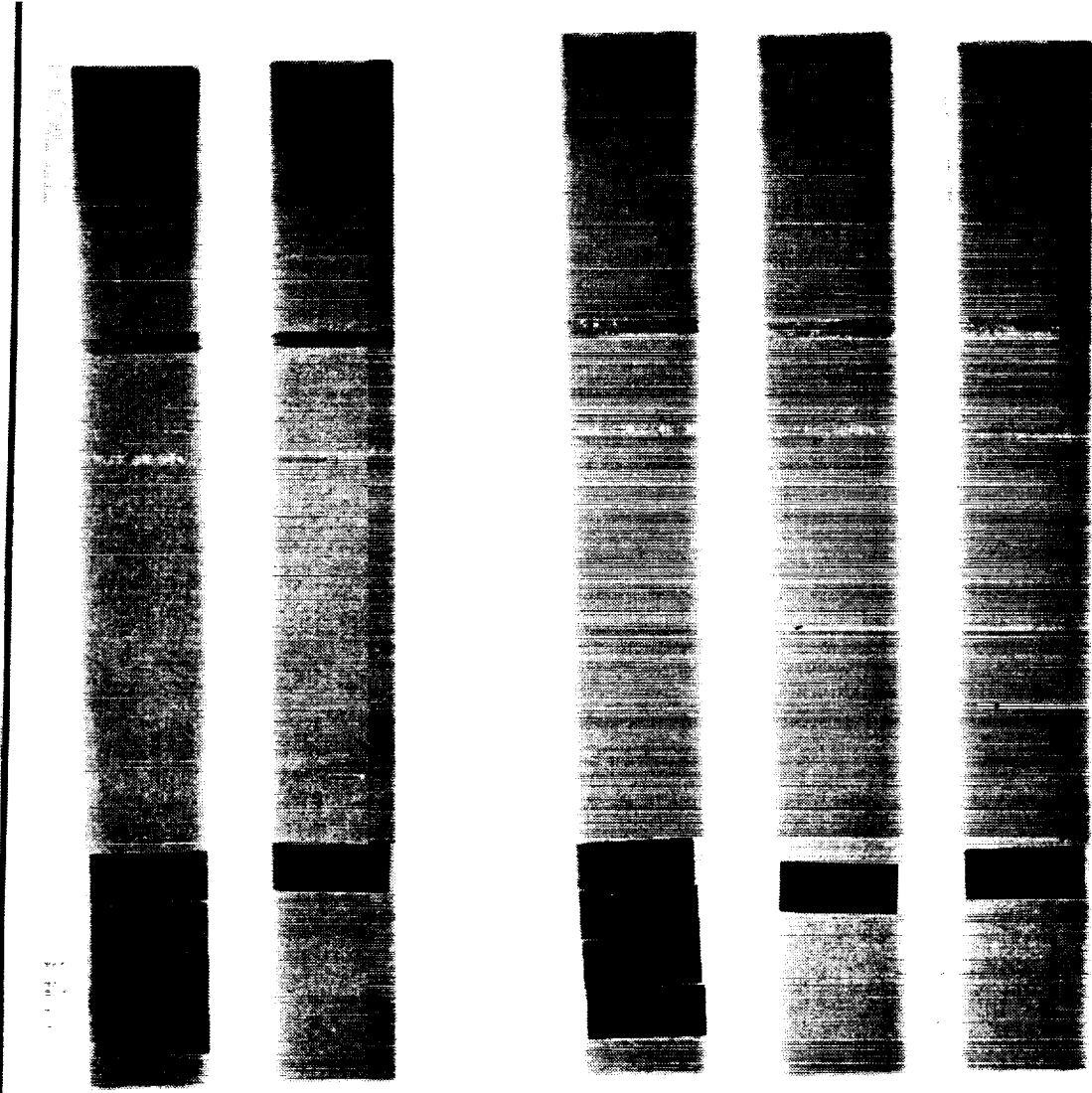Figure 11: Configuration of Weld Specimen Used to Obtain Weld Shear Strength Samples.

Figure 12: Contact Prints of Radiographs Showing Porosity in 0.050 in. (1.3 mm) Thick 8090-T6 to 0.120 in. (3.0 mm) Thick 2090-T83 weld with 0.001 in. (0.02 mm) Removed by Chemical Milling.

Figure 13: Contact Prints of Radiographs Showing Porosity in 0.050 in. (1.3 mm) Thick 8090-T6 to 0.120 in. (3.0 mm) Thick 2090-T83 weld with 0.005 in. (0.13 mm) Removed by Chemical Milling.
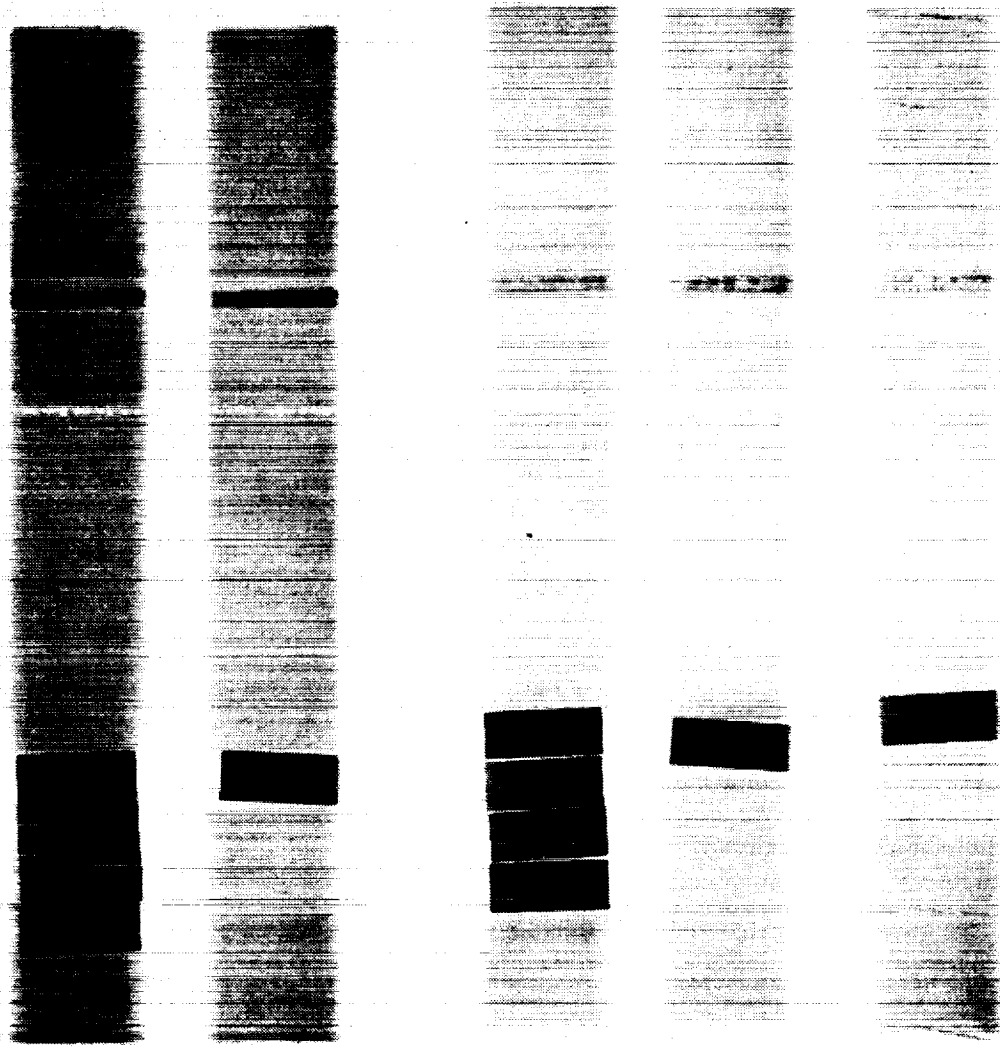
Figure 14: Contact Prints of Radiographs Showing Porosity in 0.050 in. (1.3 mm) Thick 8090-T6 to 0.120 in. (3.0 mm) Thick 2090-T83 weld with 0.010 in. (0.25 mm) Removed by Chemical Milling.

Figure 15: Contact Prints of Radiographs Showing Porosity in 0.068 in. (1.7 mm) Thick 2095-T6 to 0.120 in. (3.0 mm) Thick 2095-T8 weld with 0.001 in. (0.02 mm) Removed by Chemical Milling.

Figure 16: Contact Prints of Radiographs Showing Porosity in 0.068 in. (1.7 mm) Thick 2095-T6 to 0.120 in. (3.0 mm) Thick 2095-T8 weld with 0.005 (0.13 mm) in. Removed by Chemical Milling.

39
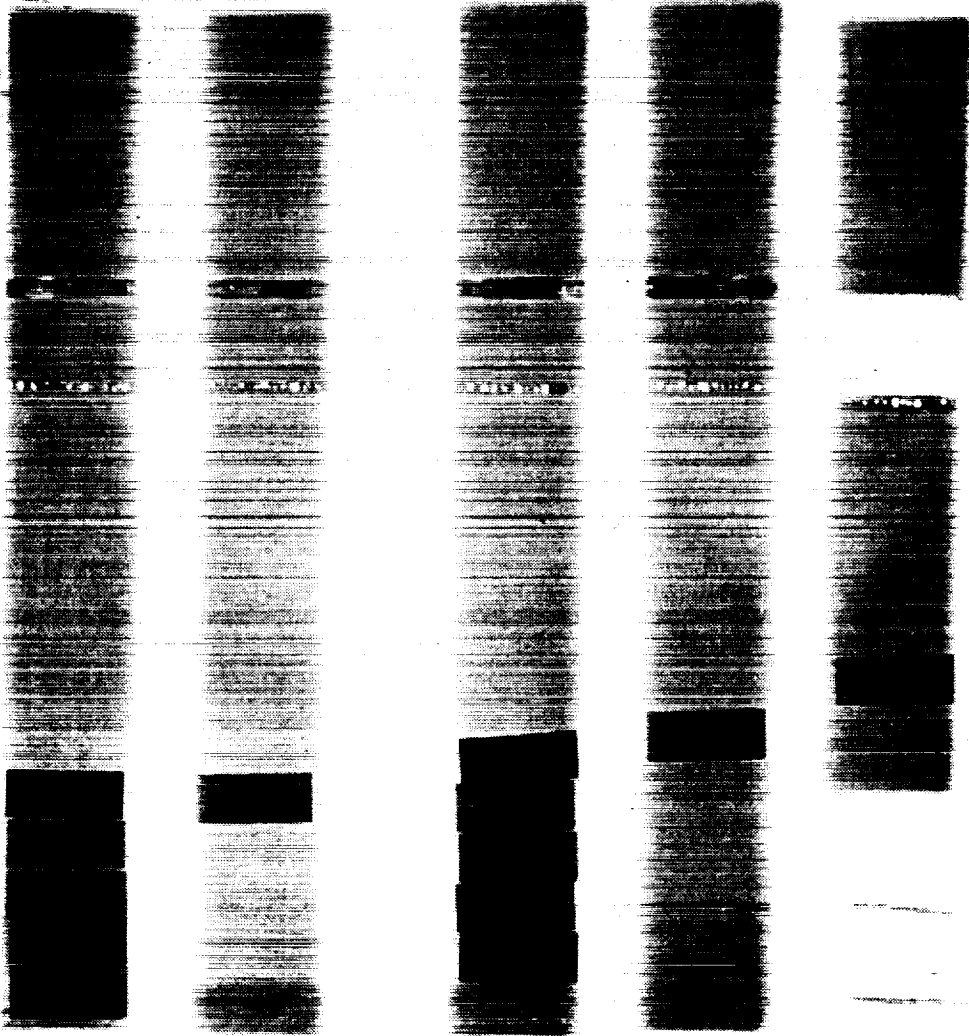
Figure 17: Contact Prints of Radiographs Showing Porosity in 0.068 in. (1.7 mm) Thick 2095-T6 to 0.120 in. (3.0 mm) Thick 2095-T8 Weld with 0.010 in. (0.25 mm) Removed by Chemical Milling.
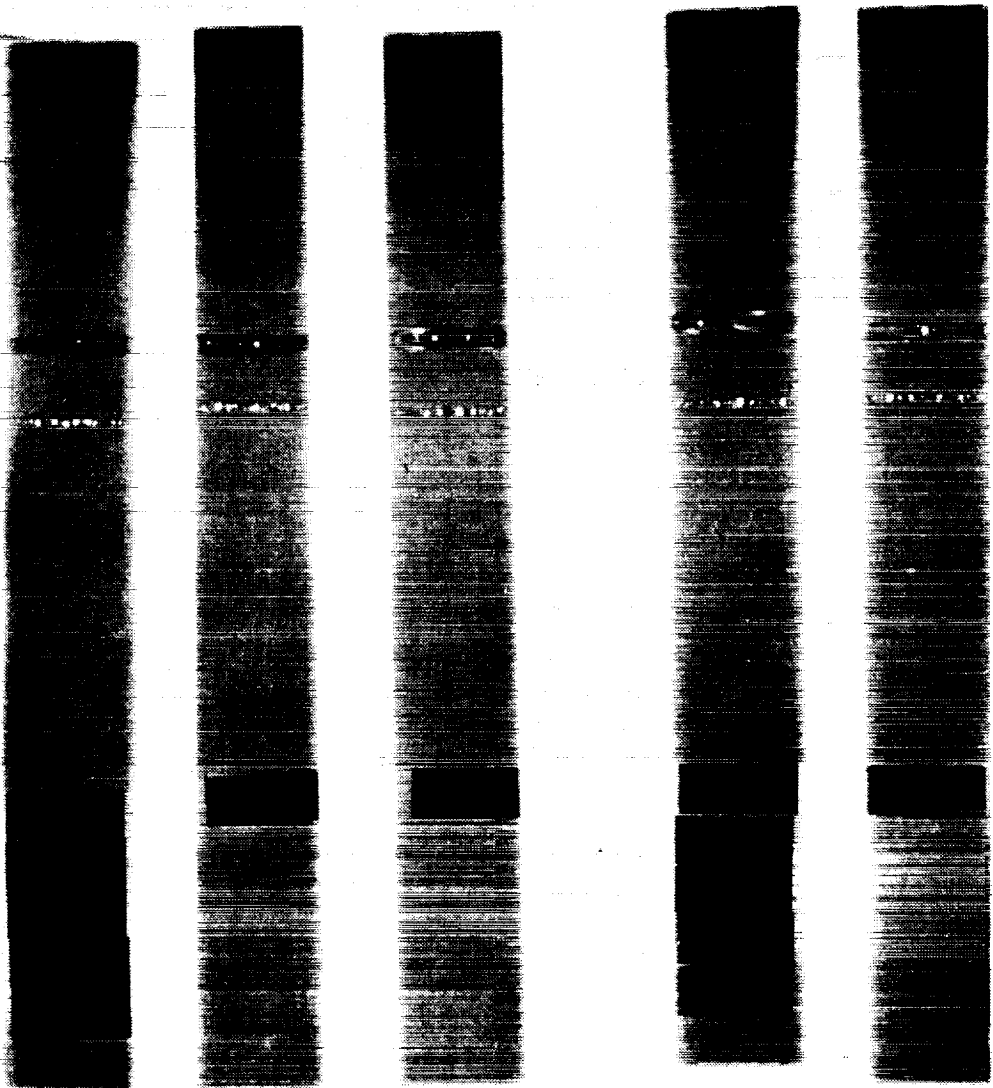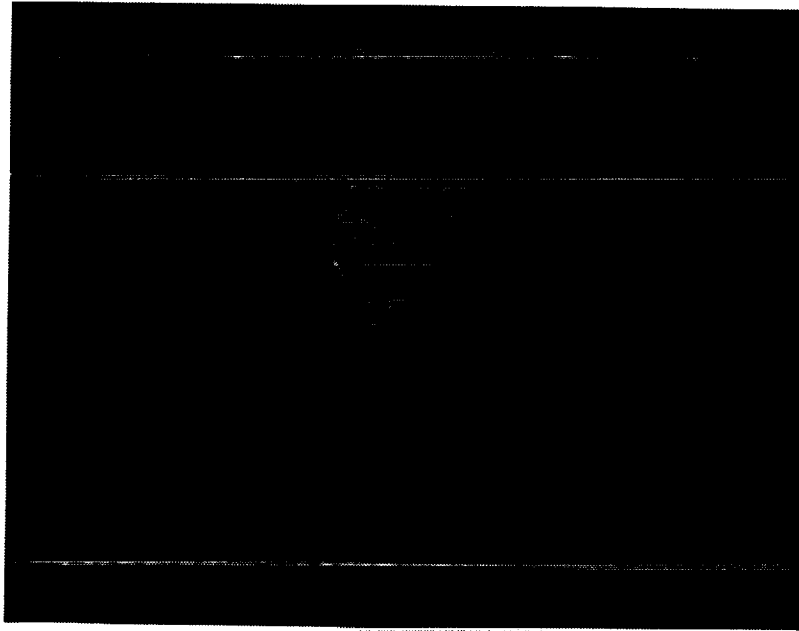
(a)

(b)
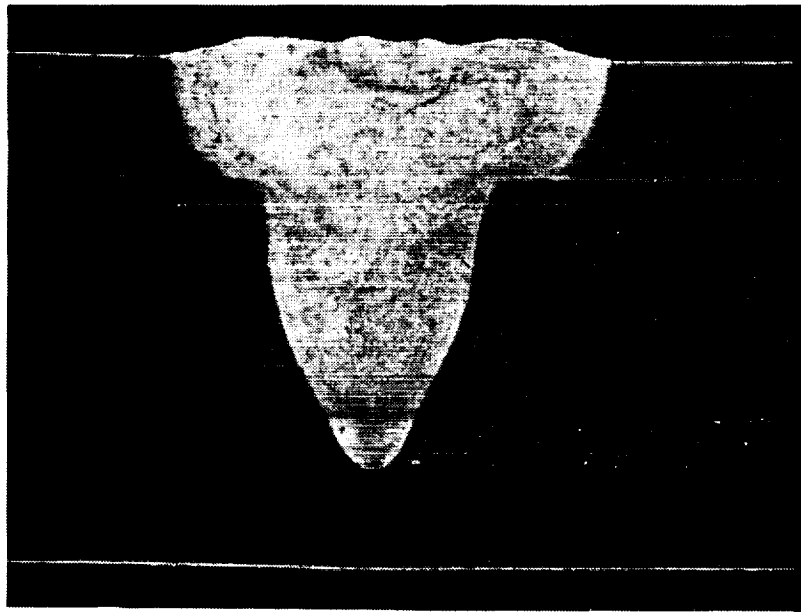
Figure 18:   Photomacrographs of Laser Beam Welds Used for
Determination of Strength Across Partial Penetration Welds
of the Face Sheet (a) 0.050 in. Thick 8090-T6 to 0.120 in.
Thick 2090-T83 and (b) 0.050 in. Thick 2095-T6 to 0.120 in. Thick
2095-T8 (Keller's Reagent).
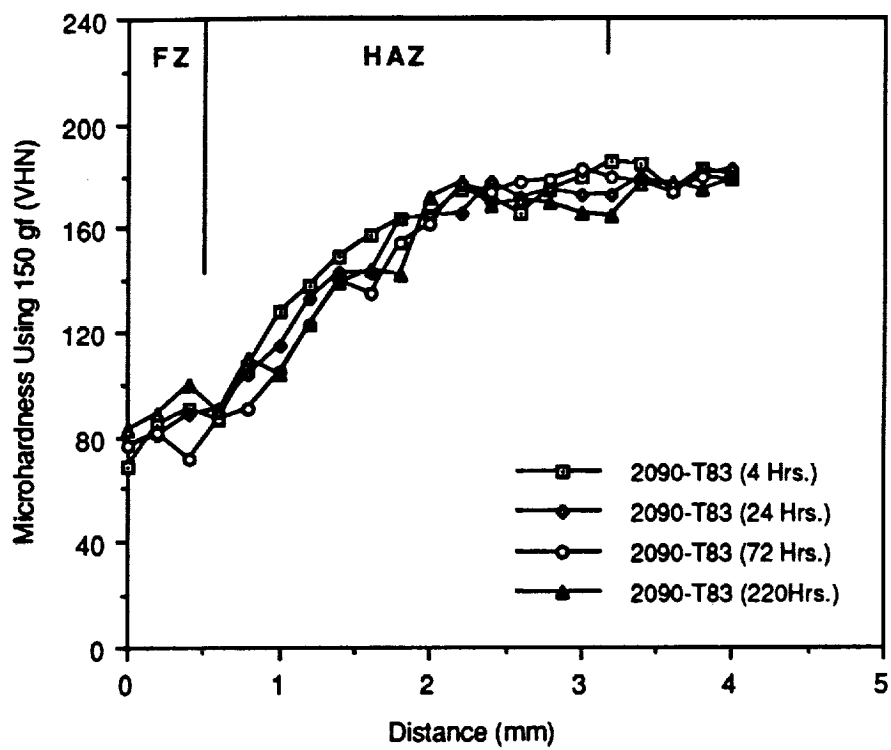
Figure 19: Hardness Profile Across Fusion Zone (FZ) and Heat Affected Zone (HAZ) of the Partial Penetration Weld in 2090-T83 at Various Times After Welding.
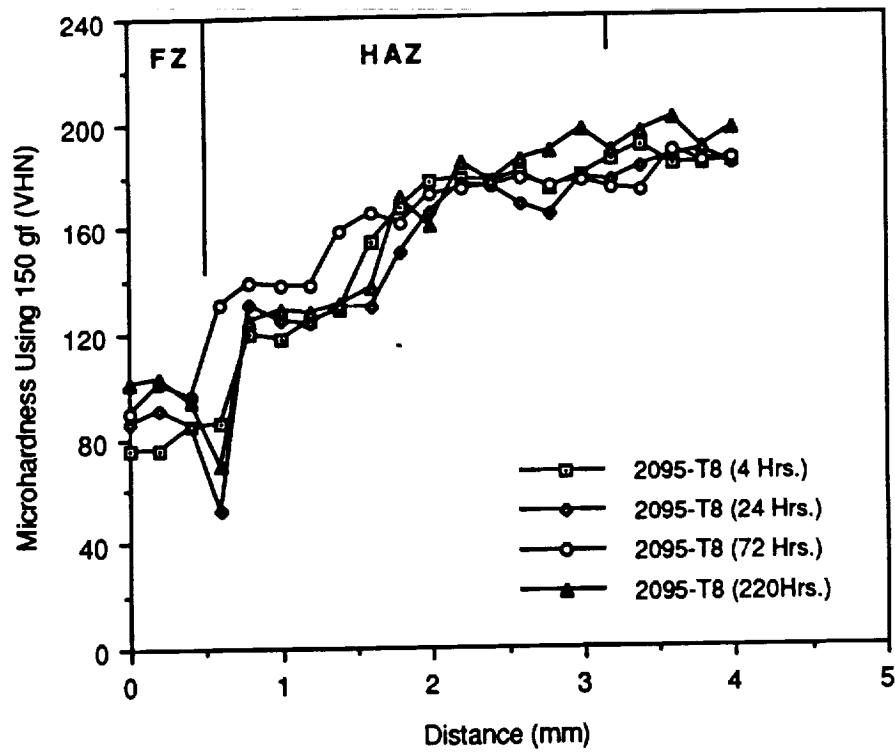
Figure 20: Hardness Profile Across Fusion Zone (FZ) and Heat Affected Zone (HAZ) of the Partial Penetration Weld in 2095-T8 at Various Times After Welding.
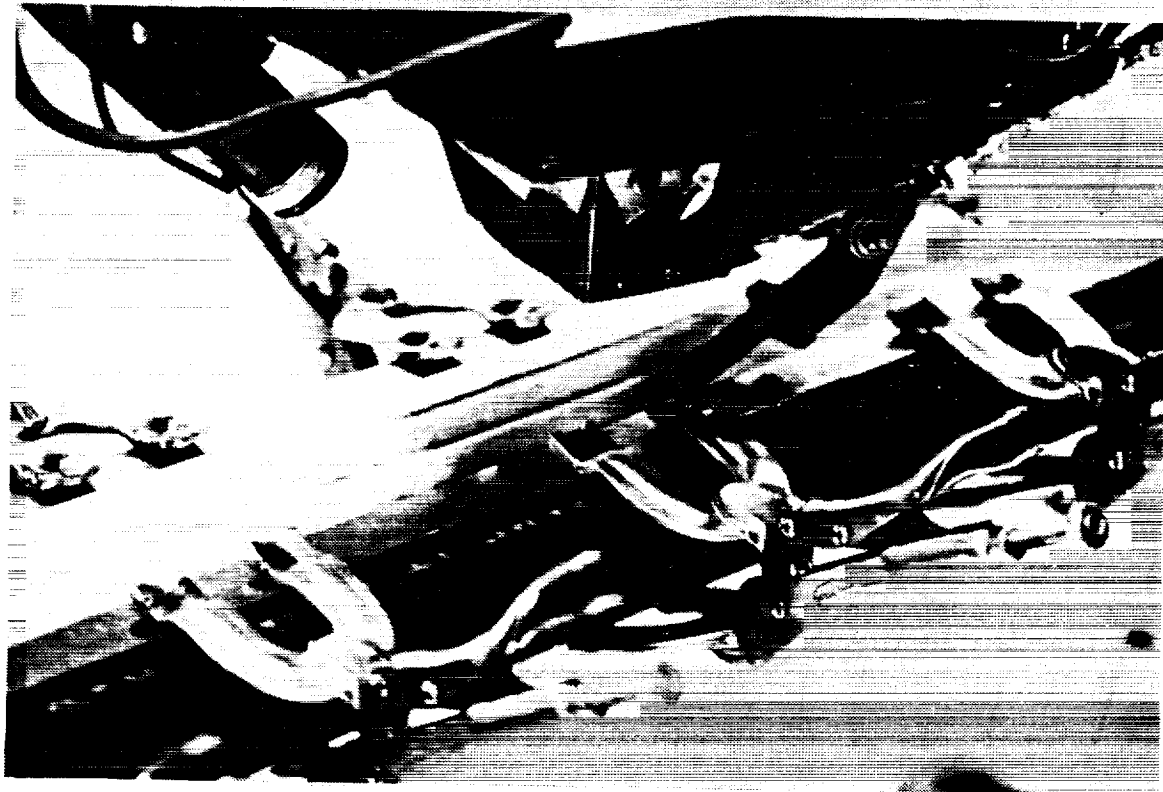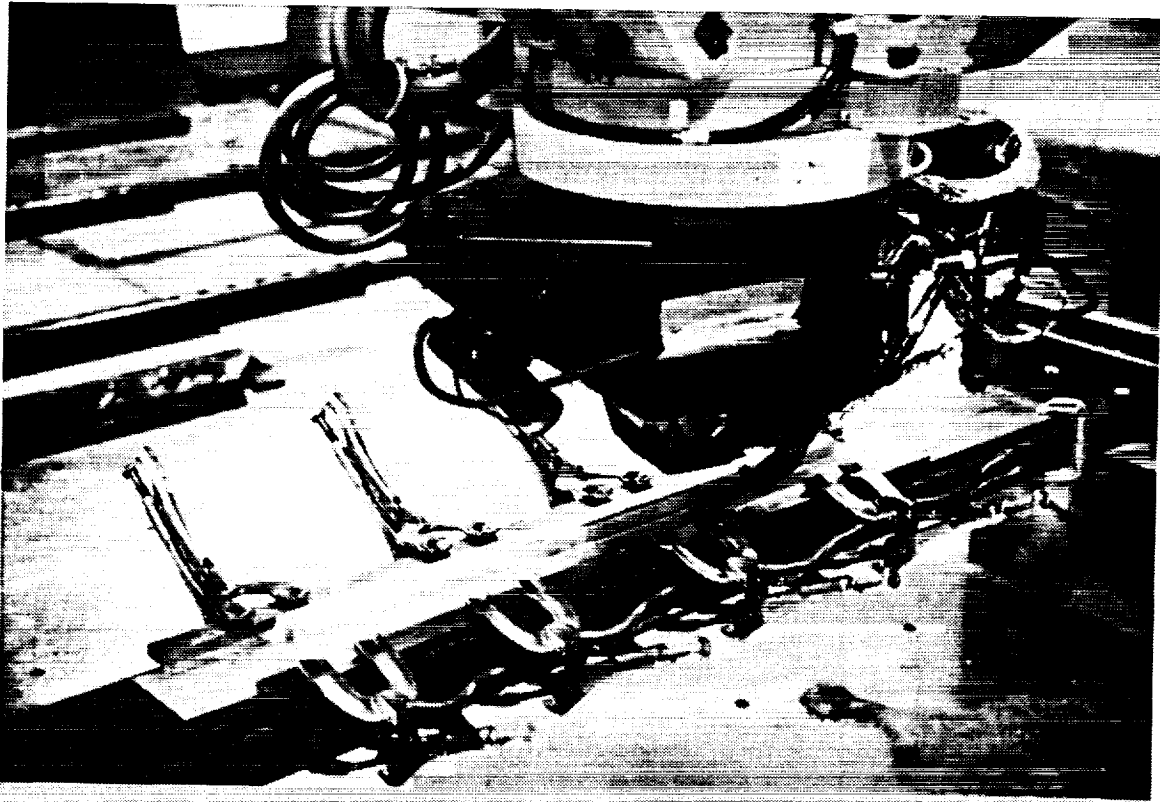
Figure 21: Photographs of Clamping Arrangement used to Weld Prototype Panels.
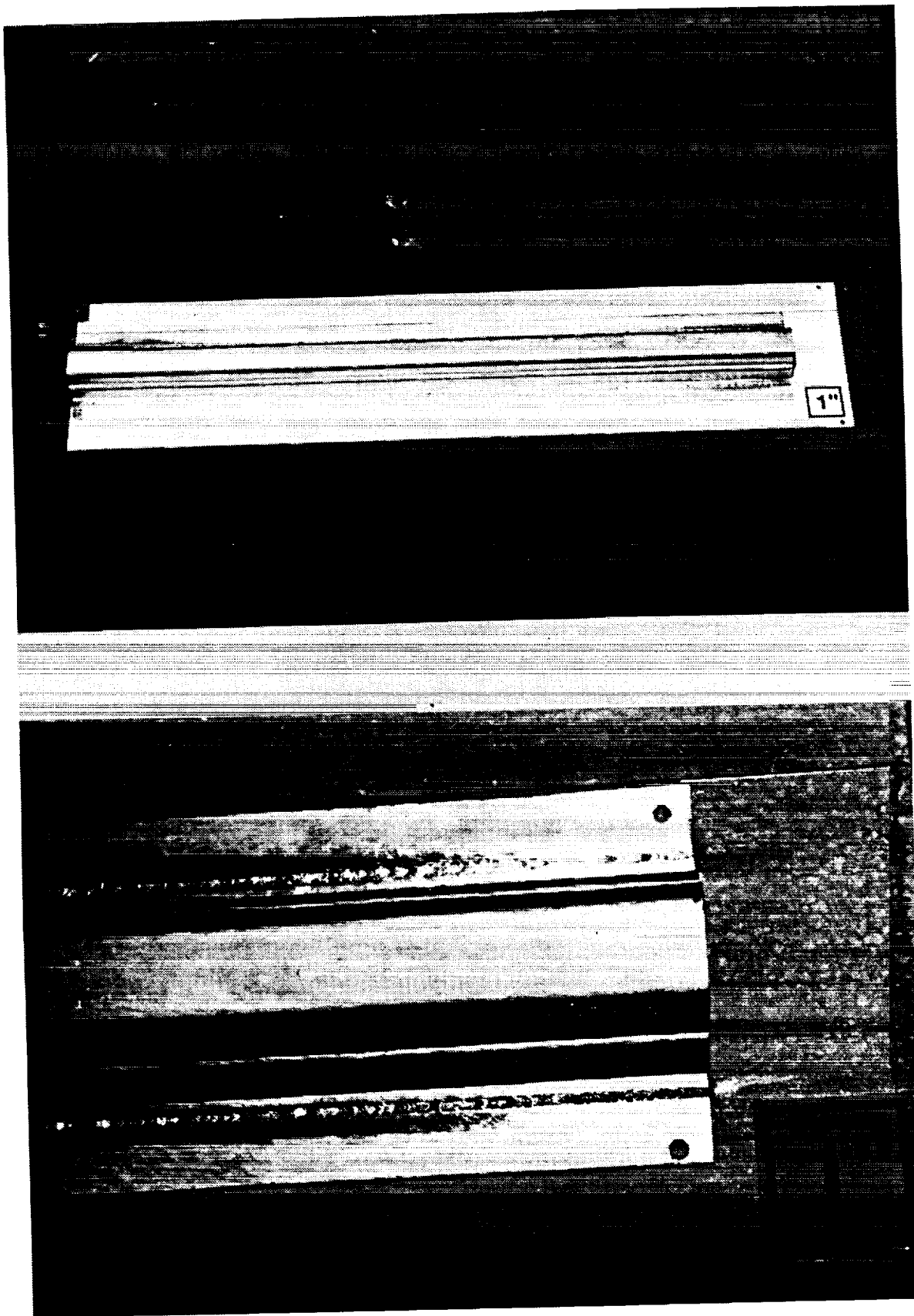
Figure 22: Photographs of a Prototype Panel that had been Laser Beam Welded.
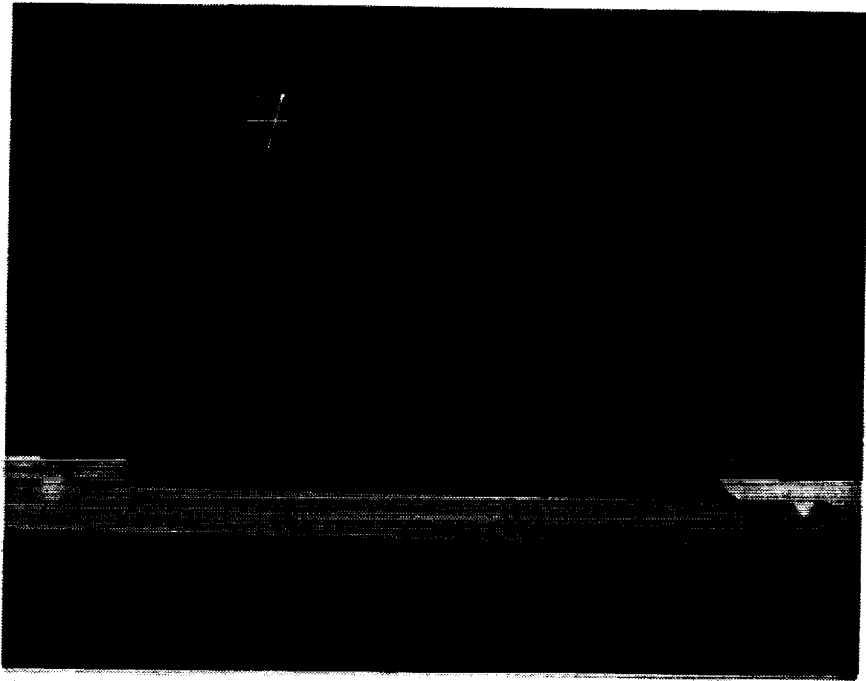
(a)

(b)

Figure 23: Macrographs of Cross-Sections of Prototype Panels: (a) 8090-T6 to 2090-T83 and (b) 2095-T6 to 2095-T8.
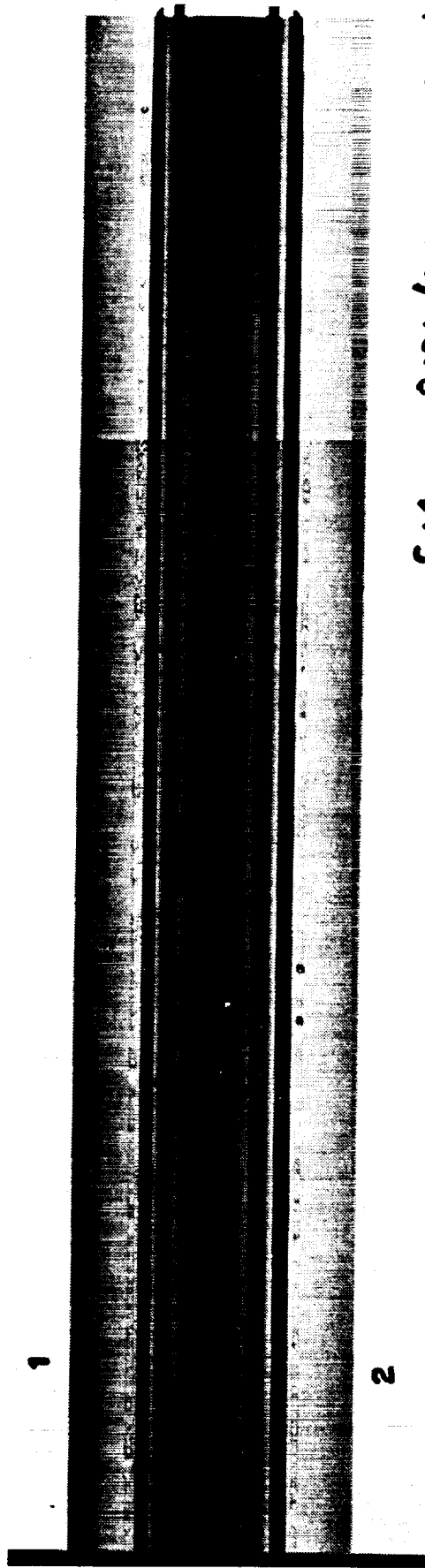
Figure 24: Contact Print of Radiograph Showing Porosity in 8090-T6 to 2090-T83 Welds on Prototype Parts That were Chemically Milled 0.001 in. (0.02 mm) Prior to Welding.
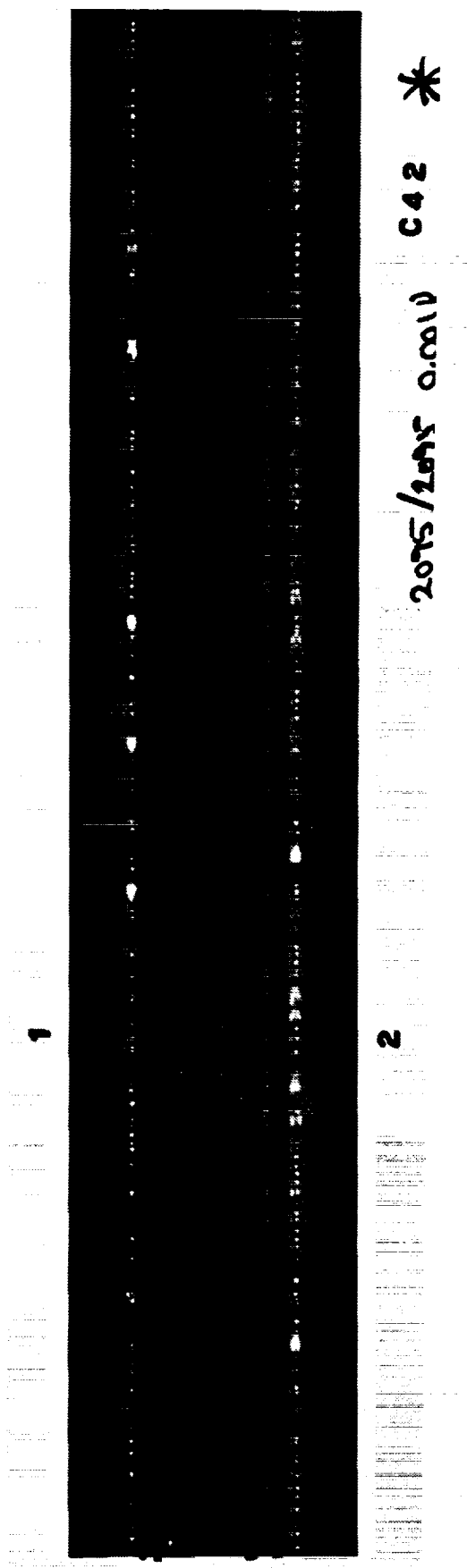
Figure 25: Contact Print of Radiograph Showing Porosity in 2095-T6 to 2095-T8 Welds on Prototype Parts That were Chemically Milled 0.001 in. (0.02 mm) Prior to Welding.
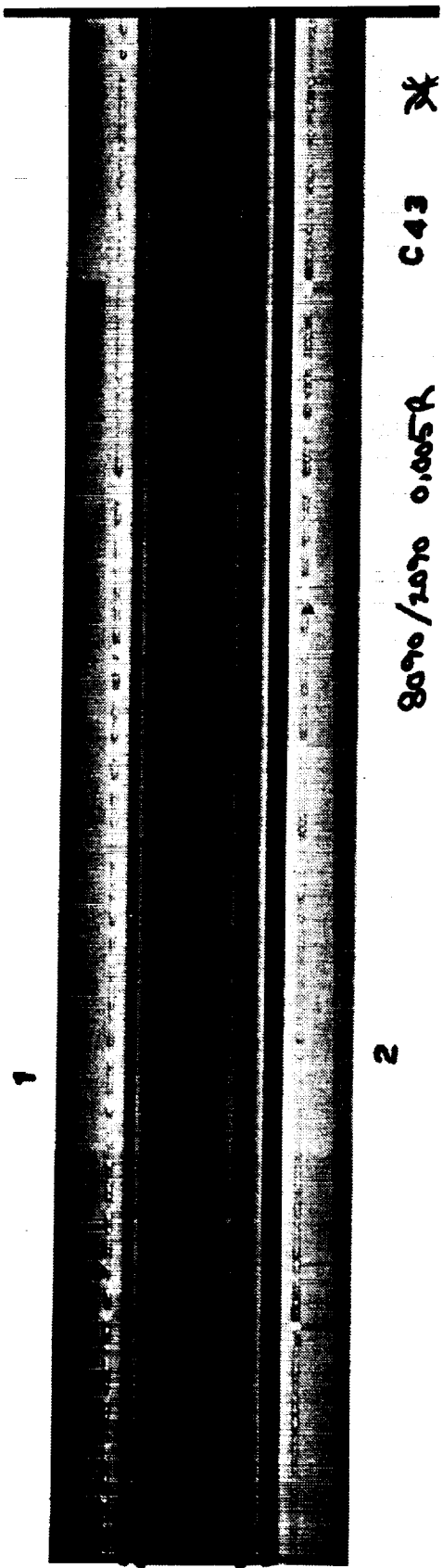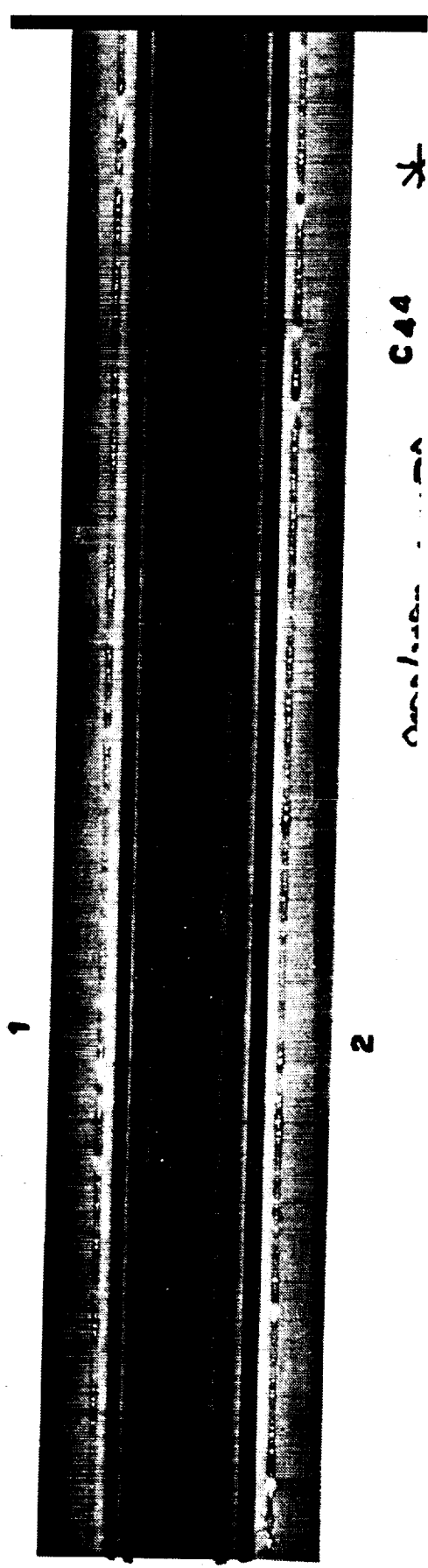
Figure 26: Contact Prints of Radiographs Showing Porosity in 8090-T6 to 2090-T83 Welds on Prototype Parts that were Chemically Milled 0.005 in. (0.13 mm) Prior to Welding.
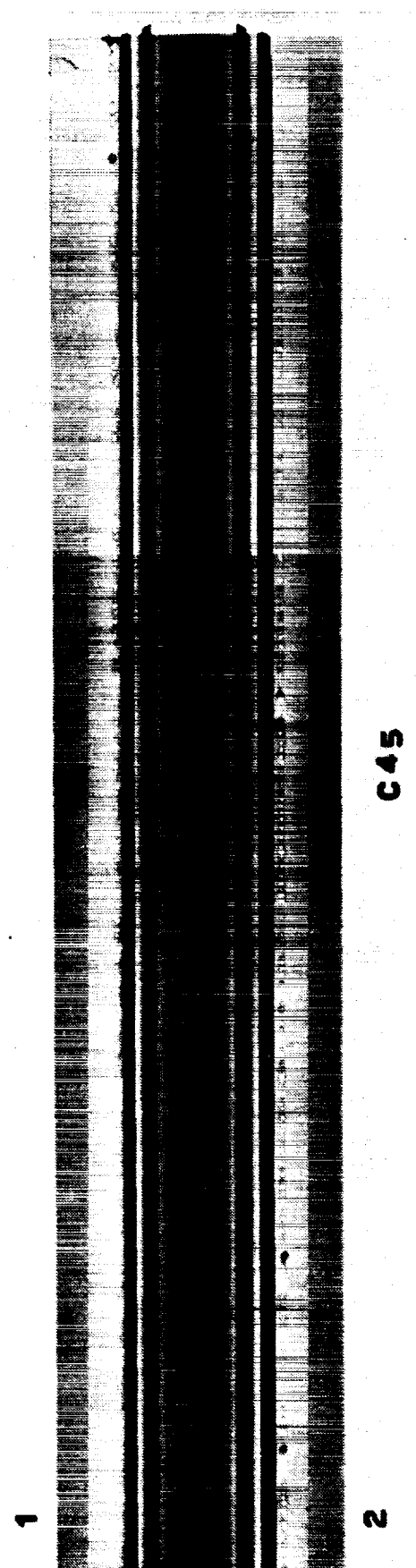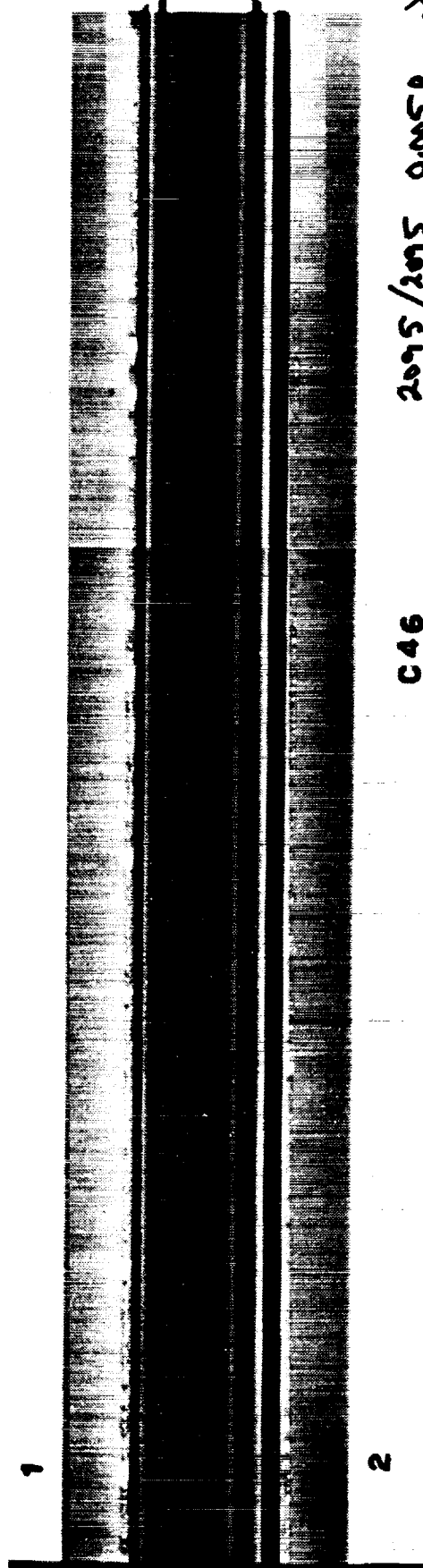
Figure 27: Contact Prints of Radiographs Showing Porosity in 2095-T6 to 2095-T8 Welds on Prototype Parts That were Chemically Milled 0.005 in. (0.13 mm) Prior to Welding.

50
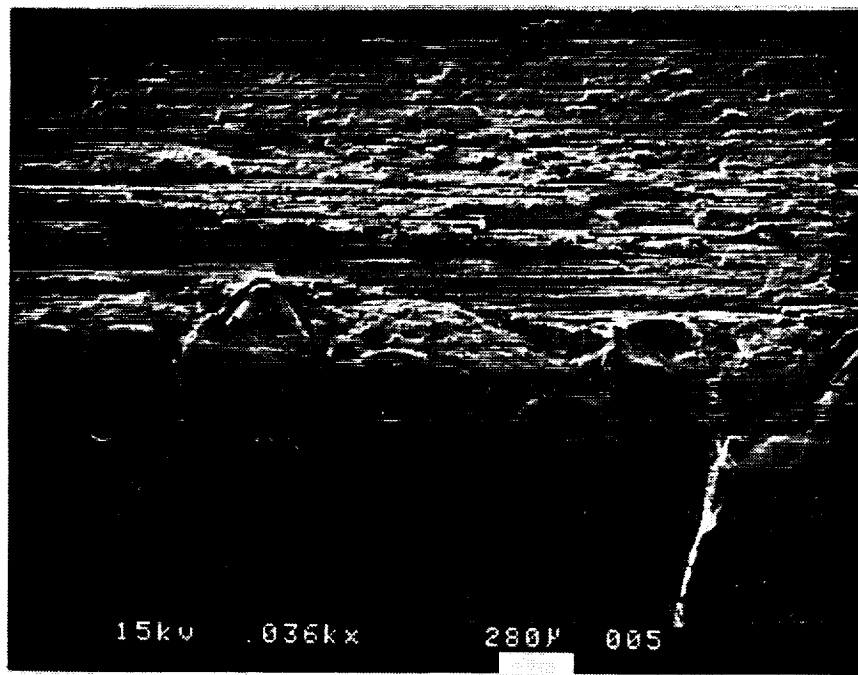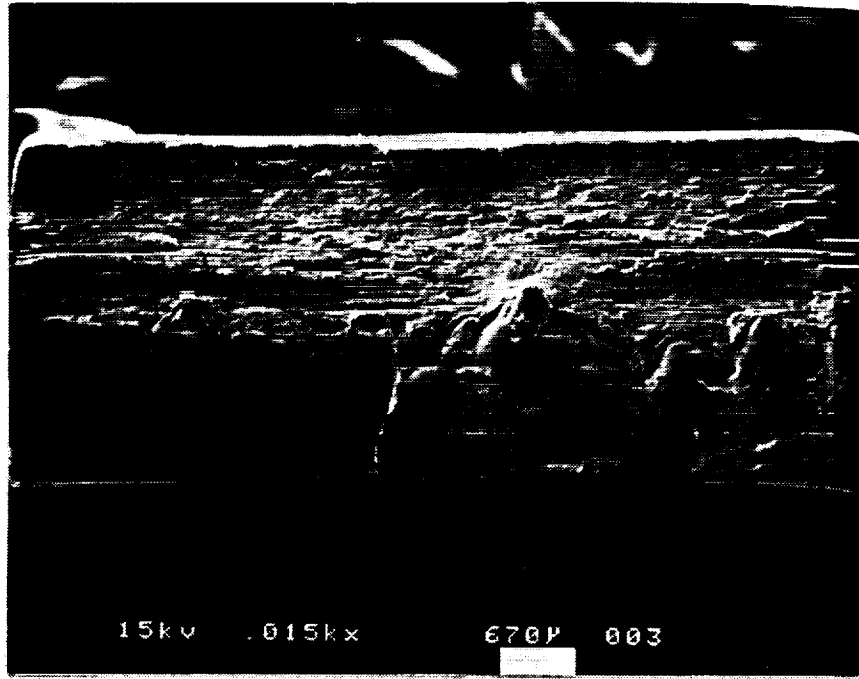
Figure 28: Scanning Electron Micrographs of Fracture Surface of Partial Penetration Welds of 2090-T83 After Tensile Testing.
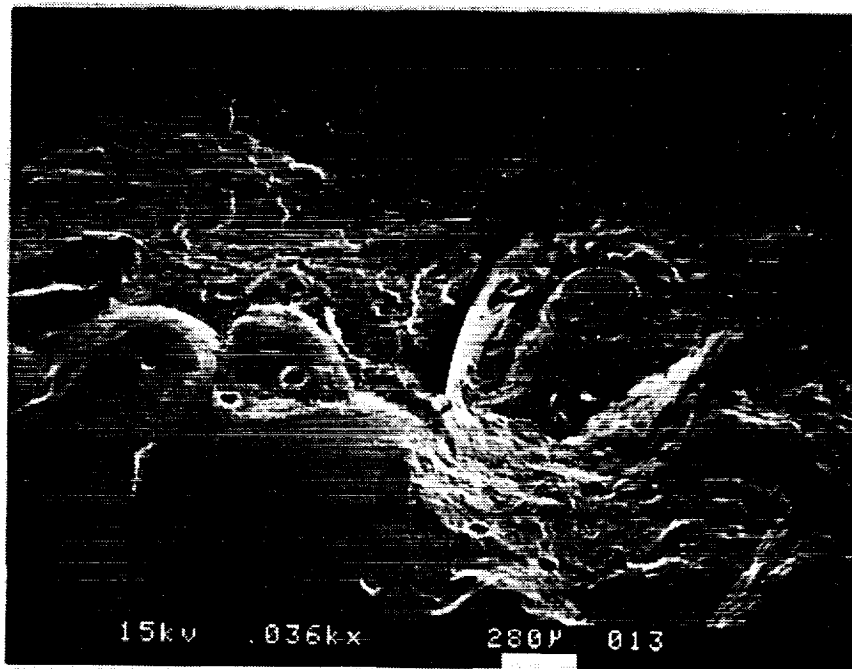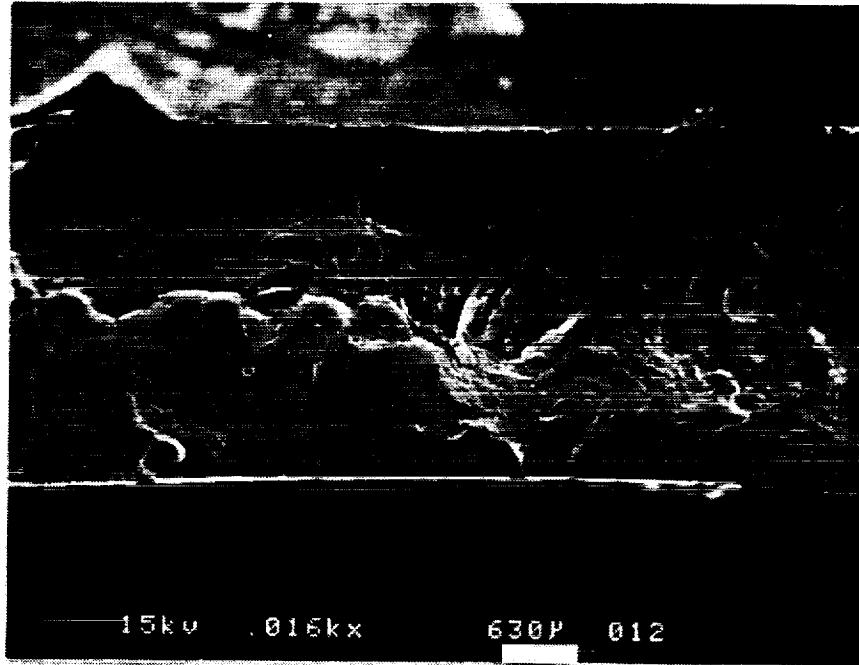
Figure 29: Scanning Electron Micrographs of Fracture Surface of Partial Penetration Welds of 2095-T8 After Tensile Testing.

52

TABLE I

Nominal Compositions, Densities, and Elastic Modulii of Aluminum-Lithium Alloys of Interest for Producing Stiffened Panels (Refs. 5-7)

wt%	8090	2090	2095
Li:	2.5	2.3	1.0
Cu:	1.0	2.7	4.0
Mg:	1.0	0.2	0.4
Zr:	0.10	0.12	0.14
Ag:	0.0	0.0	0.4
Density (gr/cm^3):	2.54	2.57	*
Elastic Modulus (GPa):	79.3	78.6	*

* Data unavailable

TABLE II

Alloy and Thickness Combinations for Stiffeners and Skin-Sheet
That Were Initially of Interest

Stiffener Alloy	Stiffener Thickness		Face-Sheet Alloy	Face-Sheet Thickness	
	in.	(mm)		in.	(mm)
8090-T6	0.050	(1.3)	2090-T83	0.095	(2.4)
8090-T6	0.050	(1.3)	2090-T83	0.120	(3.2)
2095-T6	0.050	(1.3)	2095-T8	0.095	(2.4)
2095-T6	0.050	(1.3)	2095-T8	0.120	(3.2)

TABLE III

Welding Parameters Identified During Initial Process Development

Beam Power:	6.5 to 7 kW at the source
Processing Speed:	150 to 170 IPM (6.4 to 7.2 cm/s)
Shielding Gas:	200 CFH (94.4 l/min.) Helium
Shielding Arrangement:	Helium supplied by a 0.375 in. (9.5 mm) inside-diameter nozzle at leading edge
Optical Parameters:	f10 parabolic focus lens
Stand-off Distance:	6.0 in. (15.2 cm) from work-piece to welding head

TABLE IV

Results of Factorial Experiment Showing Distribution of Porosity
(Based on the Average of Two Welds) Along With Experimental Conditions

Alloy Combination	Thickness (inches)	Pretreatment	Small Pores (<0.005 in. dia.)	Medium Pores (0.005-0.020 in. dia.)	Large Pores (>0.020 in. dia.)	Total Number of Pores
8090-T6/2090-T83	0.050 to 0.095	Chemically Cleaned	4.0	4.0	3.5	11.5
2095-T6/2095-T8	0.050 to 0.095	Chemically Cleaned	13.0	12.0	3.5	27.5
8090-T6/2090-T83	0.050 to 0.120	Chemically Cleaned	9.0	2.0	0.0	11.0
2095-T6/2095-T8	0.050 to 0.120	Chemically Cleaned	10.5	9.0	11.0	30.5
8090-T6/2090-T83	0.050 to 0.095	Wire Brushed	7.0	6.5	2.0	15.0
2095-T6/2095-T8	0.050 to 0.095	Wire Brushed	13.0	10.0	6.5	29.5
8090-T6/2090-T83	0.050 to 0.120	Wire Brushed	15.0	15.0	5.5	32.0
2095-T6/2095-T8	0.050 to 0.120	Wire Brushed	12.5	12.0	8.5	33.0

56

TABLE V

Modified Welding Parameters for Each Alloy and Thickness Combination

Alloy Combination (top sheet/bottom sheet)	Thickness Combination (inches)	Beam Power (kW)	Travel Speed (IPM)	Shielding Gas[1] (CFH)
2095-T6/2095-T8	0.050 to 0.095	6.0	150	200 He
2095-T6/2095-T8	0.050 to 0.120	6.7	150	200 He
8090-T6/2090-T83	0.050 to 0.095	5.2	160	200 He
8090-T6/2090-T83	0.050 to 0.120	5.8	160	200 He

1 Shielding gas supplied by utilizing a 0.375 in. diameter nozzle mounted at a 35° angle from the horizontal and directed at the front edge of the pool opposite the welding direction.

TABLE VI

Laser Welding Parameters Used to Produce Lap-Welds on Material That Had Been Chemically Milled by Chem-Tronic, Inc. to Remove 0.005 and 0.010 Inch Per Side

Specimen Number[1]	Alloy Combination[2] (top sheet/bottom sheet)	Thickness Combination[2] (inches)	Power (kW)	Travel Speed (IPM)	Shielding Gas [3] (CFH)
A1	8090-T6/2090-T83	0.050 to 0.095	5.2	160	200 He
A2	8090-T6/2090-T83	0.050 to 0.120	5.5	160	200 He
A4	2095-T6/2095-T8	0.050 to 0.120	7.2	150	200 He
B1	8090-T6/2090-T83	0.050 to 0.120	5.5	160	200 He
B2	8090-T6/2090-T83	0.050 to 0.095	6.0	160	200 He
B4	2095-T6/2095-T8	0.050 to 0.120	7.2	150	200 He

1 Specimens A represent 0.005 inches removed per side, and specimens B represent 0.010 inches removed per side by chemical milling.

2 Values represent actual material thickness measurements after chemical milling, and values in parentheses represent nominal starting thicknesses.

3 Shielding gas supplied utilizing a 0.375 inch inside diameter nozzle mounted at a 35° angle from the horizontal and directed at the front edge of the pool directed against the welding direction.

58

TABLE VII

Laser Beam Welding Parameters for Producing Specimens Used to Obtain Weld Shear Strength of 8090-T6 to 2090-T83

Specimen Number	Alloy Combination Top Sheet/ Bottom Sheet	Thickness Combination (in.)	Amount Removed per Side (in.)	Power (kW)	Speed (IPM)
C-1-1*	8090-T6/2090-T83	0.050 to 0.095	0.001	5.7	160
C-1-2*	8090-T6/2090-T83	0.050 to 0.095	0.001	5.3	160
C-1-3*	8090-T6/2090-T83	0.050 to 0.095	0.001	5.3	160
C-2-1*	8090-T6/2090-T83	0.050 to 0.095	0.005	5.0	160
C-2-2*	8090-T6/2090-T83	0.050 to 0.095	0.005	5.0	160
C-2-3*	8090-T6/2090-T83	0.050 to 0.095	0.005	5.0	160
C-3-1*	8090-T6/2090-T83	0.050 to 0.095	0.010	5.0	160
C-3-2*	8090-T6/2090-T83	0.050 to 0.095	0.010	5.0	160
C-3-3*	8090-T6/2090-T83	0.050 to 0.095	0.010	5.0	160
C-1-4	8090-T6/2090-T83	0.050 to 0.120	0.001	5.3	160
C-1-5	8090-T6/2090-T83	0.050 to 0.120	0.001	5.3	160
C-1-6	8090-T6/2090-T83	0.050 to 0.120	0.001	5.3	160
C-2-4	8090-T6/2090-T83	0.050 to 0.120	0.005	5.1	160
C-2-5	8090-T6/2090-T83	0.050 to 0.120	0.005	5.6	160
C-2-6	8090-T6/2090-T83	0.050 to 0.120	0.005	5.6	160
C-3-4	8090-T6/2090-T83	0.050 to 0.120	0.010	5.5	160
C-3-5	8090-T6/2090-T83	0.050 to 0.120	0.010	5.5	160
C-3-6	8090-T6/2090-T83	0.050 to 0.120	0.010	5.5	160

* Samples forwarded to NASA Langely Research Center. All other specimens retained at ARL Penn State for tension shear testing.

Note: Shielding gas supplied utilizing a 0.375 inch inside diameter nozzle mounted at a 35° angle from the horizontal and directed at the front edge of the pool directed against the welding direction.

TABLE VIII

Laser Beam Welding Parameters for Producing Specimens Used to Obtain
Weld Shear Strength of 2095-T6 to 2095-T8

Specimen Number	Alloy Combination Top Sheet/ Bottom Sheet	Thickness Combination (in.)	Amount Removed per Side (in.)	Power (kW)	Speed (IPM)
C-1-7*	2095-T6/2095-T8	0.068 to 0.095	0.001	6.0	150
C-1-8*	2095-T6/2095-T8	0.068 to 0.095	0.001	6.5	150
C-1-9*	2095-T6/2095-T8	0.068 to 0.095	0.001	6.5	150
C-2-7*	2095-T6/2095-T8	0.068 to 0.095	0.005	6.5	150
C-2-8*	2095-T6/2095-T8	0.068 to 0.095	0.005	6.2	150
C-2-9*	2095-T6/2095-T8	0.068 to 0.095	0.005	6.2	150
C-3-7*	2095-T6/2095-T8	0.068 to 0.095	0.010	6.0	150
C-3-8*	2095-T6/2095-T8	0.068 to 0.095	0.010	6.0	150
C-3-9*	2095-T6/2095-T8	0.068 to 0.095	0.010	6.0	150
C-1-10	2095-T6/2095-T8	0.068 to 0.120	0.001	6.5	150
C-1-11	2095-T6/2095-T8	0.068 to 0.120	0.001	6.5	150
C-1-12	2095-T6/2095-T8	0.068 to 0.120	0.001	6.5	150
C-2-10	2095-T6/2095-T8	0.068 to 0.120	0.005	6.3	150
C-2-11	2095-T6/2095-T8	0.068 to 0.120	0.005	6.4	150
C-2-12	2095-T6/2095-T8	0.068 to 0.120	0.005	6.4	150
C-3-10	2095-T6/2095-T8	0.068 to 0.120	0.010	6.3	150
C-3-11	2095-T6/2095-T8	0.068 to 0.120	0.010	6.3	150
C-3-12	2095-T6/2095-T8	0.068 to 0.120	0.010	6.3	150

* Samples forwarded to NASA Langely Research Center. All other specimens retained at ARL Penn State for tension shear testing.

Note: Shielding gas supplied utilizing a 0.375 inch inside diameter nozzle mounted at a 35° angle from the horizontal and directed at the front edge of the pool directed against the welding direction.

TABLE IX

Results of Tensile Tests for Base Metal and Partial Penetration Welds of 2090-T83

0.120 in. Thick 2090-T83 Partial Penetration Welds [a]				0.120 in. Thick 2090-T83 Base Metal			
Specimen ID	Ultimate Tensile Strength KSI (MPa)	Yield Strength KSI (MPa)	Elongation in 1.0 in. gage %	Specimen ID	Ultimate Tensile Strength KSI (MPa)	Yield Strength KSI (MPa)	Elongation in 1.0 in. gage %
B1-1	67.11 (462.8)	b	0	2090-1	80.59 (555.8)	75.01 (517.3)	7.0
B1-2	59.68 (411.6)	b	0	2090-2	80.23 (553.3)	74.78 (515.7)	7.0
B1-3	58.55 (403.8)	b	0	2090-3	80.43 (554.7)	74.36 (512.8)	6.0
B1-4	60.85 (419.7)	b	0				
B1-5	61.81 (426.3)	b	0				
Mean	61.60 (424.8)	c	0		80.42 (554.6)	74.7 (515.2)	6.7
Standard Deviation	3.31 (22.8)	c	0		0.177 (1.22)	0.331 (2.28)	0.6

a Lap welds produced on 0.050 in. thick 2090-T6 to 0.120 in. thick 2090-T83 at 5.5 kW power and 160 IPM travel speed. Average weld penetration of the 2090-T83 was approximately 40 percent.

b Yield strength not obtained; failed before reaching 0.2% offset.

c Mean and standard deviation not calculated.

TABLE X

Results of Tensile Tests for Base Metal and Partial Penetration Welds of 2095-T8

0.120 in. Thick 2095-T8 Partial Penetration Welds [a]				0.120 in. Thick 2095-T8 Base Metal			
Specimen ID	Ultimate Tensile Strength KSI (MPa)	Yield Strength KSI (MPa)	Elongation in 1.0 in. gage %	Specimen ID	Ultimate Tensile Strength KSI (MPa)	Yield Strength KSI (MPa)	Elongation in 1.0 in. gage %
B4-1	62.78 (433.0)	b	0	2095-1	90.22 (622.2)	84.57 (583.2)	10.0
B4-2	56.67 (390.8)	54.85 (378.3)	1.0	2095-2	89.50 (617.2)	83.79 (577.9)	10.0
B4-3	56.90 (392.4)	54.29 (374.4)	1.0	2095-3	89.92 (620.1)	84.20 (580.7)	11.0
B4-4	61.89 (426.8)	58.25 (401.7)	1.0				
B4-5	55.70 (384.1)	51.48 (355.0)	1.0				
Mean	58.79 (405.5)	54.72 (377.4)	0.8		89.88 (619.9)	84.19 (580.6)	10.3
Standard Deviation	3.28 (22.6)	2.78 (19.2)	0.4		0.36 (2.48)	0.39 (2.69)	0.6

[a] Lap welds produced on 0.050 in. thick 2095-T6 to 0.120 in. thick 2095-T8 at 7.2 kW power and 150 IPM travel speed. Average weld penetration of the 2095-T8 was approximately 60 percent.

[b] Yield strength not obtained; failed before reaching 0.2% offset.

Table XI

Results of Tension Shear Tests on 0.050 inch Thick 8090-T6 Stiffener to 0.120 inch Thick 2090-T83 Face-Sheet

Sample Number	Amount Removed per Side (in.)	Weld Length (in.)	Weld Width (in.)	Weld Area (sq.in.)	Load (lb.)	Shear Strength KSI (MPa)
C-1-4-1	0.001	0.724	0.090	0.065	902	13.9 (95.7)
C-1-4-2	0.001	0.752	0.084	0.063	802	12.7 (87.8)
C-1-5-1	0.001	0.748	0.088	0.066	755	11.4 (78.8)
C-1-5-2	0.001	0.751	0.090	0.068	823	12.1 (83.4)
C-1-5-3	0.001	0.749	0.082	0.061	733	12.0 (82.8)
C-2-5-1	0.005	0.759	0.110	0.084	950	11.3 (77.9)
C-2-5-2	0.005	0.755	0.123	0.093	926	10.0 (68.6)
C-2-6-1	0.005	0.750	0.105	0.079	904	11.4 (78.9)
C-2-6-2	0.005	0.756	0.110	0.083	907	10.9 (77.1)
C-2-6-3	0.005	0.746	0.090	0.067	860	12.8 (88.4)
C-3-4-1	0.010	0.749	0.106	0.079	879	11.1 (76.7)
C-3-4-2	0.010	0.748	0.088	0.066	717	10.9 (74.9)
C-3-4-3	0.010	0.755	0.090	0.068	643	9.5 (65.2)
C-3-5-1	0.010	0.754	0.093	0.070	878	12.5 (86.5)
C-3-5-2	0.010	0.733	0.085	0.062	765	12.3 (85.1)

Table XII

Results of Tension Shear Tests on 0.068 inch Thick 2095-T6 Stiffener to 0.120 inch Thick 2095-T8 Face-Sheet

Sample Number	Amount Removed Side (in.)	Weld Length (in.)	Weld Width (in.)	Weld Area (sq.in.)	Load (lb.)	Shear Strength KSI (MPa)
C-1-10-1	0.001	0.756	0.057	0.043	857	19.9 (137.4)
C-1-10-2	0.001	0.758	0.064	0.049	974	19.9 (137.1)
C-1-10-3	0.001	0.754	0.066	0.050	987	19.7 (136.1)
C-1-12-1	0.001	0.754	0.062	0.047	1003	21.3 (147.1)
C-1-12-2	0.001	0.756	0.065	0.049	955	19.5 (134.3)
C-2-11-1	0.005	0.756	0.065	0.049	997	20.4 (140.3)
C-2-11-2	0.005	0.759	0.066	0.050	942	18.8 (129.9)
C-2-11-3	0.005	0.754	0.066	0.050	933	18.7 (128.6)
C-2-12-1	0.005	0.755	0.070	0.053	797	15.0 (103.6)
C-2-12-2	0.005	0.752	0.066	0.050	984	19.7 (135.7)
C-3-10-1	0.010	0.756	0.060	0.045	976	21.7 (149.5)
C-3-10-2	0.010	0.740	0.070	0.052	1005	19.3 (133.2)
C-3-11-1	0.010	0.757	0.065	0.049	892	18.2 (125.5)
C-3-11-2	0.010	0.760	0.065	0.049	888	18.1 (124.9)
C-3-11-3	0.010	0.760	0.065	0.049	941	19.2 (132.4)

Table XIII

Parameters for Laser Beam Welding of Prototype Panels
(0.050 in. Thick Stepped-Hat Stiffeners to 0.120 in. Face-Sheet)

Amount Removed per Side (in.)	Alloy Combination	Prototype Part Number		Travel Speed (IPM)	Beam Power (kW)	Estimated Percent Penetration
0.001	8090-T6 to 2090-T83	C-4-1	Weld 1	160	5.3	0
			Weld 2	160	5.7	50
0.001	2095-T6 to 2095-T8	C-4-2	Weld 1	150	6.3	70
			Weld 2	150	6.3	50
0.005	8090-T6 to 2090-T83	C-4-3	Weld 1	160	5.2	10
			Weld 2	160	5.2	25
0.005	8090-T6 to 2090-T83	C-4-4	Weld 1	160	5.8	50
			Weld 2	160	5.8	30
0.005	2095-T6 to 2095-T8	C-4-5	Weld 1	150	6.3	90
			Weld 2	150	6.3	50
0.005	2095-T6 to 2095-T8	C-4-6	Weld 1	150	6.3	60
			Weld 2	150	6.3	45

65

REPORT DOCUMENTATION PAGE

Public reporting burden for this collection of information is estimated to average 1 hour per response, including the time for reviewing instructions, searching existing data sources, gathering and maintaining the data needed, and completing and reviewing the collection of information. Send comments regarding this burden estimate or any other aspect of this collection of information, including suggestions for reducing this burden, to Washington Headquarters Services, Directorate for Information Operations and Reports, 1215 Jefferson Davis Highway, Suite 1204, Arlington, VA 22202-4302, and to the Office of Management and Budget, Paperwork Reduction Project (0704-0188), Washington, DC 20503.

1. AGENCY USE ONLY (Leave blank)	2. REPORT DATE April 1993	3. REPORT TYPE AND DATES COVERED Contractor Report

4. TITLE AND SUBTITLE

The Feasibility of Producing Aluminum-Lithium Structures for Cryogenic Tankage Applications by Laser Beam Welding

6. AUTHOR(S)

R. P. Martukanitz
K. G. Lysher

5. FUNDING NUMBERS

L-4409D

505-63-50-03

7. PERFORMING ORGANIZATION NAME(S) AND ADDRESS(ES)

Applied Research Laboratory
The Pennsylvania State University
P.O. Box 30
State College, PA 16804

8. PERFORMING ORGANIZATION REPORT NUMBER

TM 93-067

9. SPONSORING / MONITORING AGENCY NAME(S) AND ADDRESS(ES)

National Aeronautics and Space Administration
Langley Research Center
Hampton, VA 23681-0001

10. SPONSORING / MONITORING AGENCY REPORT NUMBER

NASA CR-191527

11. SUPPLEMENTARY NOTES

12a. DISTRIBUTION / AVAILABILITY STATEMENT

12b. DISTRIBUTION CODE

13. ABSTRACT (Maximum 200 words)

Aluminum-lithium alloys exhibit high strength, high elastic modulus, and low density as well as excellent cryogenic mechanical properties making them ideal material candidates for cryogenic tanks. NASA has proposed the use of "built-up" structure for panels fabricated into cryogenic tanks replacing current conventional machining. Superplastically formed stiffeners would be joined to sheet (tank skin) that had been roll formed to the radius of the tank in order to produce panels. Aluminum-lithium alloys of interest for producing the built-up structure include alloy 2095-T6 stiffeners to 2095-T8 sheet and alloy 8090-T6 stiffeners to 2090-T83 sheet.

Laser welding, with comparable joint properties, offers the following advantages over conventional welding: higher production rates, minimal degradation within the heat affected zones, and full process automation. This study established process parameters for laser beam welding, mechanical property determinations, metallographic characterization, and fabrication of prototype panels.

Tensile tests representing partial penetration of the skin alloys provided joint efficiencies between 65 and 77 percent, depending upon alloy and degree of penetration. Results of tension shear tests of lap welds indicated that the combination of 2095-T6 to 2090-T8 exhibited significantly higher weld shear strength at the interface in comparison to welds of 8090-T6 to 2090-T83. The increased shear strength associated with 2095 is believed to be due to the alloy's ability to precipitation strengthen (naturally age) after welding.

14. SUBJECT TERMS

Laser Welding
Aluminum-lithium alloys (2090, 8090, 2095)
Built-up structure

15. NUMBER OF PAGES

73

16. PRICE CODE

A04

17. SECURITY CLASSIFICATION OF REPORT	18. SECURITY CLASSIFICATION OF THIS PAGE	19. SECURITY CLASSIFICATION OF ABSTRACT	20. LIMITATION OF ABSTRACT
UNCLASSIFIED	UNCLASSIFIED		